β-catenin drives distinct transcriptional networks in proliferative and non-proliferative cardiomyocytes.

Gregory A. Quaife-Ryan[1,2], Richard J. Mills[1], George Lavers[1], Holly K. Voges[3], Celine J. Vivien[3], David A. Elliott[3,4,5], Mirana Ramialison[4], James E. Hudson[1,*], Enzo R. Porrello[3,6,*,#].

[1]*QIMR Berghofer Medical Research Institute, Herston, Brisbane, Queensland, 4006, Australia.*

[2]*School of Biomedical Sciences, The University of Queensland, St Lucia, Brisbane, Queensland, 4072, Australia*

[3]*Murdoch Children's Research Institute, The Royal Children's Hospital, Parkville, Victoria, 3052, Australia.*

[4]*Australian Regenerative Medicine Institute, Monash University, Clayton, Victoria, 3800, Australia.*

[5]*Department of Paediatrics, The Royal Children's Hospital, University of Melbourne, Parkville, Victoria, 3052, Australia.*

[6]*Department of Physiology, School of Biomedical Sciences, The University of Melbourne, Parkville, Victoria, 3010, Australia.*

[*]*Co-corresponding authors.*

[#]Lead contact.

Please address correspondence to:

Enzo R. Porrello, PhD
Murdoch Children's Research Institute
The Royal Children's Hospital
Parkville, Victoria, 3052, Australia
enzo.porrello@mcri.edu.au

James E. Hudson
QIMR Berghofer Medical Research Institute
Herston, Brisbane, 4006, Australia
james.hudson@qimrberghofer.edu.au

Keywords: cardiac regeneration, cardiomyocyte proliferation, Wnt/beta-catenin, transcriptional regulation, metabolism

Summary Statement

β-catenin is repurposed from pro-proliferative to protective functions in cardiomyocytes during postnatal heart development.

Abstract

The inability of the adult mammalian heart to regenerate represents a fundamental barrier in heart failure management. In contrast, the neonatal heart retains a transient regenerative capacity, but the underlying mechanisms for the developmental loss of cardiac regenerative capacity in mammals are not fully understood. Wnt/β-catenin signaling has been proposed as a key cardio-regenerative pathway driving cardiomyocyte proliferation. Here, we show that Wnt/β-catenin signaling potentiates neonatal mouse cardiomyocyte proliferation *in vivo* and immature human pluripotent stem cell-derived cardiomyocyte (hPSC-CM) proliferation *in vitro*. In contrast, Wnt/β-catenin signaling in adult mice is cardioprotective but fails to induce cardiomyocyte proliferation. Transcriptional profiling and chromatin immunoprecipitation sequencing of neonatal mouse and hPSC-CM revealed a core Wnt/β-catenin-dependent transcriptional network governing cardiomyocyte proliferation. In contrast, β-catenin failed to re-engage this neonatal proliferative gene network in the adult heart despite partial transcriptional re-activation of a neonatal glycolytic gene program. These findings suggest that β-catenin may be repurposed from regenerative to protective functions in the adult heart in a developmental process dependent on the metabolic status of cardiomyocytes.

Introduction

For over 30 years it has been recognised that cardiomyocyte proliferation is shutdown during early postnatal development of the mammalian heart (Rumyantsev and Borisov, 1987; Soonpaa et al., 1996). As proliferative potential is lost, cardiomyocytes undergo maturation, whereby fetal/neonatal genes encoding structural, cell cycle and metabolic proteins are exchanged for mature adult transcriptional programs to meet the functional demands of postnatal life (Taegtmeyer et al., 2010). Hence, the global transition from an immature to a mature state involves changes in almost every facet of cardiomyocyte physiology, including loss of cardiomyocyte proliferative potential. However, the molecular processes that govern the transitions from hyperplastic to hypertrophic growth remain poorly characterised. Following MI in adult mammals (where ~25% of cardiomyocytes perish), the very low basal rate of adult cardiomyocyte turnover (<1%) is insufficient to restore damaged cardiomyocytes and recover heart function (Bergmann et al., 2015). Alternatively, during the first days of life when cardiomyocytes are actively proliferating, neonatal mammals possess a robust, albeit transient capacity for cardiac regeneration (Porrello et al., 2011; Ye et al., 2018; Zhu et al., 2018). Therefore, understanding and modulating the processes by which cardiomyocytes mature and cease proliferating in the postnatal window could lead to potential therapies for heart failure patients.

A host of postnatally regulated factors have been linked to the loss of cardiomyocyte proliferative capacity including cyclins and cyclin-dependent kinases (Mohamed et al., 2018), tumour-suppressors (Sdek et al., 2011), transcription factors (Heallen et al., 2011; Mahmoud et al., 2013), microRNAs (Eulalio et al., 2012; Porrello et al., 2013), growth factor receptors (D'Uva et al., 2015), hormones (Hirose et al., 2019), vagal innervation (Mahmoud et al., 2015), metabolic substrates (Mills et al., 2017), immune factors (Aurora et al., 2014; Natarajan et al., 2018), extracellular matrix components (Bassat et al., 2017), epigenetic programming (Quaife-Ryan et al., 2017), and the oxidative postnatal environment (Nakada et al., 2017). Although modulation of these processes stimulates cardiomyocyte proliferation, none completely regenerate the adult heart after MI.

We previously undertook an extensive multicellular transcriptional analysis of the neonatal and adult mouse heart to identify drivers of cardiac regeneration and uncovered a possible role for Wnt/β-catenin signaling (Quaife-Ryan et al., 2017). We subsequently screened pro-proliferative factors in human pluripotent stem cell-derived cardiac organoids (hCO) *in vitro*

and discovered that β-catenin signaling was repressed during cardiac maturation (Mills et al., 2017). Although the contribution of Wnt/β-catenin to neoplastic diseases is well-characterised, confusion exists surrounding the exact role of β-catenin in the postnatal heart. Contradictory evidence suggests β-catenin drives adult cardiomyocyte hypertrophy (Chen et al., 2006; Hahn et al., 2006) or adult cardiomyocyte hyperplasia (Iyer et al., 2018) and can be cardioprotective (Hahn et al., 2006) or facilitate pathological cardiac remodelling (Iyer et al., 2018). Moreover, cardiac regenerative pathways, such as Hippo/Yap, insulin-like growth factor, peroxisome proliferator-activated receptor delta and neuregulin/Erbb2, co-opt β-catenin signaling to stimulate cardiomyocyte proliferation (D'Uva et al., 2015; Heallen et al., 2011; Magadum et al., 2017; Xin et al., 2011). Similarly, Wnt/β-catenin signaling induces immature hPSC-CMs and neonatal human atrial cardiomyocytes to proliferate *in vitro* (Mills et al., 2017; Wang et al., 2016), whereas other studies suggest that β-catenin is only activated in cardiomyocytes of human failing hearts (Hou et al., 2016). Wnt/β-catenin signaling is activated in several cell types post-infarction (cardiomyocytes, endothelial cells, leukocytes, Sca-1+/c-Kit+ progenitor cells, and fibroblasts) (Oerlemans et al., 2010). However, the cell type-specific functions of Wnt/β-catenin signalling in these diverse cardiac cell populations have not been fully elucidated. Hence, Wnt/β-catenin function appears to be highly context dependent and its role in cardiomyocyte proliferation and maturation remains poorly delineated.

Here, we demonstrate that β-catenin augments proliferation of immature neonatal mouse cardiomyocytes and immature hPSC-CMs. In contrast, β-catenin deploys a cardioprotective response in the adult heart that is independent of cardiomyocyte proliferation. The adult cardioprotective response is associated with partial transcriptional reversion towards an immature cardiomyocyte metabolic state. This study also shows that β-catenin drives distinct transcriptional programs associated with proliferative networks in regenerative cardiomyocytes and immunomodulatory networks in non-regenerative adult cardiomyocytes. Hence, β-catenin stimulates immature cardiomyocyte proliferation but is unable to drive adult cardiac regeneration. Finally, it is proposed that pro-proliferative factors, such as β-catenin, may be repurposed from proliferative to protective functions in the adult heart in a process dependent on the metabolic status of cardiomyocytes.

Results

Wnt/β-catenin signaling drives a core proliferative transcriptional program in human PSC-derived cardiomyocytes

The neonatal regenerative window in mice and pigs closes within the first week of postnatal development (Porrello et al., 2011; Ye et al., 2018; Zhu et al., 2018). Recent comparison of the neonatal and adult cardiac transcriptomes suggests that Wnt/β-catenin signaling is postnatally shutdown concomitant with the closing of the regenerative window (Quaife-Ryan et al., 2017). Consistent with this finding, nuclear expression of active β-catenin (phosphorylated-Y489) was reduced during postnatal development of the mouse heart between P1 and P7 and was virtually undetectable in P14 cardiomyocytes (Fig. 1A). Moreover, the total expression of *Ctnnb1* and the main transcriptional effector of β-catenin, *Tcf7l2*, were also downregulated between P1 and P14 (Fig. 1B). These results suggest that the shutdown of postnatal Wnt/β-catenin activity correlates with the loss of regenerative potential during heart development.

Wnt/β-catenin signaling was previously identified as a driver of hPSC-CM proliferation (Mills et al., 2017). In particular, the GSK3 inhibitor, CHIR99021 (CHIR), was identified as a potent cardiomyocyte mitogen in immature hPSC-CM. We therefore sought to determine whether β-catenin is required to facilitate CHIR-induced cardiomyocyte proliferation in immature hCO (Fig. 1C). β-catenin has pleiotropic actions in the cell-cell cadherin junction and directs transcriptional responses by migrating into the nucleus. CHIR stimulated accretion of total β-catenin at intercalated disks but also increased nuclear localisation of active β-catenin (Fig. 1D,E). Similar to what was observed in mouse cardiomyocytes *in vivo*, *CTNNB1* was down regulated during human development (Fig. 1F). CHIR also lead to an increase in cardiomyocyte proliferation in hCO as evidenced by increased Ki-67 and pH3 staining (Fig. 1G,H).

We next investigated whether CHIR stimulated cardiomyocyte proliferation though β-catenin. Because hCO contain both cardiomyocytes and stromal cells (Mills et al., 2017; Voges et al., 2017), the cardiomyocyte-specific effects of CHIR were assessed using an *NKX2-5*^{eGFP} cell line followed by FACS purification of cardiomyocytes (GFP+) and stromal cells (GFP-). *NKX2-5*^{eGFP} hCO were treated with DMSO or CHIR and the purity of isolated cell populations was validated by qPCR for *COL1A1* and *MYH6* (Fig. 1J,K). Using *AXIN2* as

a read-out for β-catenin transcriptional activity, it was determined that CHIR increased *AXIN2* expression in hCO cardiomyocytes (Fig. 1L). The small molecule, iCRT-14, inhibits the interaction between β-catenin and its transcriptional effector partner, TCF7L2 (Gonsalves et al., 2011). When hCO were treated with CHIR and iCRT-14, *AXIN2* expression and Ki-67 staining were blunted (Fig. 1M,N). These results indicate that CHIR promotes cardiomyocyte cell-cycle activity through β-catenin/TCF7L2-depedent signaling.

To define the transcriptional networks regulated by canonical Wnt/β-catenin signaling in immature hPSC-CM, we subjected purified hPSC-CM and CD90+ stromal cells treated with CHIR to RNA-seq. CHIR significantly regulated 1244 genes in cardiomyocytes, 689 genes in CD90+ stromal cells and co-regulated a network of 299 genes in both myocytes and stromal cells (Fig. 2A). In cardiomyocytes and stromal cells, CHIR down-regulated specific transcriptional programs controlling cell identity such as cardiac muscle contraction and heart development in cardiomyocytes and cell matrix adhesion and regulation of cell migration in CD90+ stromal cells (Fig. 2B,C). CHIR induced a common suite of cell-cycle related transcriptional programs in both cell populations (Fig. 2C). Collectively, these findings suggest that CHIR stimulates β-catenin/TCF7L2 signaling to drive partial loss of cellular identity whilst simultaneously promoting cell proliferation. Despite partial loss-of cellular identity, principal coordinate analysis demonstrated that CD90+ stromal cells and cardiomyocytes remained transcriptionally distinct even after CHIR treatment (Fig. S1).

To ascertain which genes were the direct targets of β-catenin in human cardiomyocytes, ChIP-seq of TCF7L2 in CHIR-stimulated hPSC-CMs was performed (Fig. 2D). Enhancers and promoters of cardiomyocytes were also identified using ChIP-seq of H3K27ac and H3K4me3 histone marks, respectively. Pearson correlation of ChIP-seq indicated a high degree of reproducibility between replicates, however, only peaks present in both samples were retained for subsequent analyses (Fig. 2E,F). As would be expected for enhancers, H3K27ac predominantly labelled loci >5kb from the closest TSS (Fig. 2G). GREAT analysis suggested that these H3K27ac labelled enhancers were closest to genes associated with response to stress and cardiovascular system development (Fig 2G). Alternatively, H3K4me3 peaks were located proximal to TSSs and as expected predominantly decorated gene promoters, which were associated with metabolic processes and cell-cycle regulation (Fig. 2G). H3K27ac and H3K4me3 ChIP-seq was further validated by assessing peak location at well-characterised cardiomyocyte promoters and enhancers (Fig. S2). β-catenin has previously been shown to predominantly bind to enhancers rather than promoters in

cardiomyocytes (Iyer et al., 2018). In concordance with this finding, TCF7L2 peaks were located distant to TSS and occupied genes associated with glycosylphosphatidylinositol synthesis and nucleogenesis (Fig. 2G and Fig. S3). DNA-binding motif analysis indicated TCF/LEF motifs as the most enriched binding sites in the isolated TCF7L2-enhancer and TCF7L2-promoter peaks, thus validating the TCF7L2-ChIP-seq dataset (Fig. 2H,I). These TCF7L2-occupied enhancers and promoters were associated with BMP-signaling, mitochondrial replication and Wnt receptor signaling by BMP pathway (Fig. 2J).

Next, the core β-catenin gene network was identified by isolating CHIR-regulated genes that were also direct targets of TCF7L2 in hPSC-CM s (Fig. 2K). Upregulated direct targets of β-catenin were strongly associated with cell-cycle. Downregulated genes were associated with hypoxia response and the β-catenin destruction complex (Fig. 2K).

Wnt/β-catenin function is contingent on cardiomyocyte maturity during mouse development.

During the first week of life, neonatal cardiomyocyte proliferation is rapidly shutdown (Alkass et al., 2015). Delivery of cardiac mitogens during this period markedly augments cardiomyocyte proliferation presumably because neonatal cardiomyocytes are in a proliferative state (D'Uva et al., 2015; Heallen et al., 2011). To determine whether Wnt/β-catenin drives cardiomyocyte proliferation in the neonatal cardiomyocyte proliferative window, a constitutively active form of β-catenin called N90Δ-CTNNB1 (caBCAT) was delivered to neonatal mice using adeno-associated virus-6 (AAV6-caBCAT)(Fig. 3A). Cardiomyocyte BrdU incorporation was markedly increased in caBCAT injected mice (Fig. 3B,C). Although heart weight was unaltered (Fig. 3D), the cross-sectional area of caBCAT-treated cardiomyocytes was significantly reduced (Fig. 3E). Moreover, cardiomyocyte number was increased by ~16% in caBCAT treated neonatal mice (Fig. 3F), consistent with *bona fide* induction of cardiomyocyte proliferation. Echocardiographic assessment of caBCAT treated mice indicated that fractional shortening was slightly increased when compared to controls although ejection fraction was unaffected (Fig. 3G). To determine whether endogenous Wnt/β-catenin was required for neonatal cardiomyocyte proliferation *in vivo*, neonatal mice were treated with IWR-1, which stabilises the β-catenin destruction complex and thereby inhibits Wnt/β-catenin signaling (Chen et al., 2009). IWR-1 treatment significantly reduced cell-cycle activity in the neonatal mouse heart as indicated by pH3

staining (Fig. 3H). Hence, Wnt/β-catenin signaling potentiates neonatal cardiomyocyte proliferation during the first week of postnatal development in mice.

β-catenin was demonstrated to drive both neonatal mouse and immature hPSC-CM proliferation, but the adult heart is refractory to cardiomyocyte mitogens (Quaife-Ryan et al., 2016). We therefore assessed whether caBCAT was capable of potentiating adult cardiomyocyte proliferation in an adult mouse MI model (Fig. 4A). AAV6-caBCAT was benchmarked against the well-characterised pro-proliferative mitogen, YAP1 (Lin et al., 2014). For these experiments a constitutively active form of YAP1, called YAP1-S127A (caYAP), was encapsulated in AAV6. Characterisation of AAV6 intracardiac injections showed transgene expression specifically at intracardiac injection sites and strong enrichment for gene expression in cardiomyocytes (Fig. S4). Both caBCAT and caYAP exhibited marked cardioprotective effects on cardiac function (Fig. 4B). Moreover, caBCAT significantly mitigated cardiac scarring following MI compared to GFP controls (Fig. 4C,D). FACS quantification of fibroblasts, leukocytes, and endothelial cells at day 3 post-MI indicated that caBCAT expression diminished fibroblast number (Fig. S5), suggesting that the β-catenin antifibrotic response is instructed during the early reparative phase post infarction. However, in contrast to caYAP which increased BrdU incorporation and exerted anti-hypertrophic effects in adult cardiomyocytes (Fig. 4E,G,H), caBCAT exerted similar cardioprotective effects independently of cardiomyocyte proliferation as neither BrdU incorporation nor pH3 were elevated compared to controls (Fig. 4F,G,H). Hence, Wnt/β-catenin potentiates proliferation of immature hPSC-CMs and neonatal mouse cardiomyocytes, but is insufficient to drive proliferation of adult cardiomyocytes despite its cardioprotective actions in the adult myocardium.

To understand how β-catenin facilitated cardioprotection rather than regeneration in the adult heart, RNA-seq was performed on cardiomyocytes isolated from caBCAT or GFP-treated adult mice following MI (Fig. 5A). Principal coordinate analysis suggested good reproducibility between replicates (Fig. 5B). It was previously demonstrated that adult fibroblasts and leukocytes revert to a neonatal-like transcriptional state following MI, whereas adult cardiomyocytes do not (Quaife-Ryan et al., 2017). Hence, we next assessed whether β-catenin could facilitate the acquisition of a neonatal-like transcriptional program in adult cardiomyocytes. Comparison of the caBCAT and GFP transcriptional signatures with a previously published transcriptional resource of neonatal and adult mouse cardiomyocytes following MI (Quaife-Ryan et al., 2017) revealed that neither group fully

reverted to a neonatal-like transcriptional state post-MI (Fig. S6). However, a subset of caBCAT downregulated genes were associated with mitochondrial biogenesis, oxidative phosphorylation and the Warburg effect, as well as the beta-adrenergic hypertrophic response (*Ppargc1a*, *Nr4a3*, and *Cebpb*) (Arany et al., 2005; Bhalla et al., 2014; Feng et al., 2015; Pearen et al., 2008) (Fig. 5C). *Klf15*, a known negative regulator of β-catenin signaling (Noack et al., 2012), was also downregulated by caBCAT treatment. Gene ontological analysis revealed caBCAT downregulated genes were associated with catecholamine stimulus and regulation of transcription (Fig. 5D). Interestingly, caBCAT appeared to induce inflammatory, angiogenic and apoptotic transcriptional responses in adult cardiomyocytes (Fig. 5D). Therefore, caBCAT stimulates a cardioprotective response associated with modulation of oxidative phosphorylation and inflammatory genes without inducing cell-cycle transcriptional networks in adult cardiomyocytes.

Understanding the differential Wnt/β-catenin response in regenerative and non-regenerative cardiomyocytes.

Wnt/β-catenin signaling has distinct functions in proliferative cardiomyocytes (immature hPSC-CMs and neonatal myocytes) and non-proliferative cardiomyocytes (adult myocytes). To understand the context-dependent role of β-catenin during development, the β-catenin transcriptional response of proliferative myocytes and adult myocytes was compared. We first compared target genes of TCF7L2, CHIR-responsive genes and a published network of cardio-regenerative genes (Quaife-Ryan et al., 2017) (Fig. 6A). A core network of 21 genes were shared in common between these data sets. The CHIR-response and cardio-regenerative gene network displayed significant overlap with 32.9% of the cardio-regenerative genes also regulated by CHIR (Fig. 6A). On the other hand, the CHIR-responsive and adult myocyte caBCAT responses were largely transcriptionally distinct (4.3% of MIP56.caBCAT genes were present in the CHIR dataset) (Fig. 6B).

We next validated whether the core CHIR-regenerative network genes were downregulated when β-catenin signaling was inhibited in neonatal mouse hearts *in vivo* using IWR-1 (Fig. 6C). qPCR confirmed downregulation of a number of genes in the core CHIR-proliferative network following IWR-1 inhibition of β-catenin signaling in neonatal mice (Fig. 6C). These β-catenin target genes were highly downregulated in adult versus neonatal mouse cardiomyocytes (Fig. 6D). In contrast, the same set of genes was unaffected in adult hearts treated with caBCAT (Fig. 6C). It has been previously shown that the capacity of β-catenin

to bind to its targets is partially dependent on the epigenetic status of target gene loci (Li et al., 2011; Wöhrle et al., 2007). However, the promoter regions of core genes in the CHIR-regenerative transcriptional network did not become progressively inaccessible during postnatal development (Fig. S7). Hence, the differential role of β-catenin in immature and mature cardiomyocytes appears to be facilitated by distinct gene programs, which cannot be explained by the loss of chromatin accessibility at cardio-regenerative target loci.

Discussion

During postnatal development, cardiomyocytes undergo drastic transcriptional changes that result in cell-cycle arrest and, as a result, the adult heart becomes largely insensitive to mitotic stimuli (Gilsbach et al., 2018). Our previous multicellular transcriptomic analysis of mammalian heart regeneration predicted a core β-catenin-dependent transcriptional network associated with the neonatal cardiac regenerative state (Quaife-Ryan et al., 2017). Based on these findings, it was hypothesised that β-catenin signaling may be central to neonatal cardiomyocyte proliferation and it was further proposed that reinduction of Wnt/β-catenin signaling could promote adult cardiomyocyte proliferation. Here, we demonstrate that the role of β-catenin is highly dependent on the developmental maturity of cardiomyocytes. β-catenin potentiated proliferation of immature cardiomyocytes but lead to cardioprotection in the adult heart following MI without inducing cardiomyocyte proliferation.

The transcriptional targets of Wnt/β-catenin signaling in specific cardiac cell populations are not well defined. To further characterise Wnt/β-catenin-dependent transcriptional networks in human cardiac cells, we transcriptionally profiled hPSC-CMs and stromal cells following GSK3 inhibition with CHIR. As would be expected, canonical Wnt/β-catenin signaling was characterised by induction of a core network of cell cycle-related genes common to both cardiomyocytes and CD90+ stromal cells. However, β-catenin signaling also elicited distinct gene programs in these cell types suggesting that the β-catenin transcriptional response is partially dependent on cellular identity. Moreover, CHIR-treated cardiomyocytes exhibited diminished sarcomeric gene expression whereas CHIR-treated stromal cells displayed decreased expression of cell adhesion/ECM genes, consistent with partial loss of cell identity. Downregulation of contractile genes in cardiomyocytes treated with CHIR is consistent with previous observations that GSK3 inhibition diminishes cardiac contractility in hCO and knockout mice (Mills et al., 2017; Zhou et al., 2016). Notably, GSK3 inhibition in hPSC-CMs treated with CHIR induced ~35% of the neonatal mouse regenerative gene

network identified in Quaife-Ryan et al[21]. A core subset of 20 of these genes were also direct targets of β-catenin/TCF7L2 identified by ChiP-seq. Importantly, pharmacological inhibition of β-catenin in neonatal mice was associated with repression of several genes embedded within this core network. Overall, these findings define a common transcriptional program through which β-catenin promotes proliferation of immature human and mouse cardiomyocytes.

A key finding of the current study is that β-catenin has divergent roles in immature and mature cardiomyocytes. β-catenin failed to promote adult cardiomyocyte proliferation but engendered a cardioprotective response and ameliorated scar size following MI. The transcriptional responses of immature and mature cardiomyocytes to active β-catenin signaling displayed strikingly minimal overlap. Only ~5% of adult β-catenin-regulated genes were also direct targets of β-catenin in hPSC-CMs. Moreover, these adult β-catenin-responsive genes were not differentially regulated by β-catenin inhibition in the neonatal mouse heart. Therefore, Wnt/β-catenin signaling is repurposed during postnatal cardiac development. Interestingly, this phenomenon occurs without changes in chromatin accessibility around the promoters of β-catenin target genes during postnatal cardiomyocyte maturation. One possibility is that β-catenin is redirected from regenerative to cardioprotective gene targets by complexing with distinct transcription factor binding partners in immature and mature cardiomyocytes. Future studies could validate this contention by identifying protein binding partners of nuclear localised β-catenin in neonatal and adult myocytes. Another possibility is that β-catenin-responsive enhancers are repurposed from pro-regenerative to protective functions during mammalian development as has been recently reported for regeneration-responsive enhancers in zebrafish and killifish (Wang et al., 2020).

In contrast to the proliferative gene networks activated by β-catenin in immature cardiomyocytes, β-catenin promotes cardioprotection in the adult heart after MI without stimulating cardiomyocyte proliferation. In contrast, it should be noted that other studies have reported that Wnt/β-catenin signaling drives fibrosis in the adult heart by promoting ECM deposition from cardiac fibroblasts (Duan et al., 2012; Zhao et al., 2015). Our studies utilised AAV6, which is highly cardiomyocyte-specific (Fig. S4). We show that cardiomyocyte-specific expression of β-catenin is protective and that the anti-fibrotic effects of AAV6-BCAT likely occur secondary to cardioprotective effects in cardiomyocytes. Transcriptional analysis of caBCAT-treated adult hearts suggested that β-catenin signaling

was associated with modulation of genes involved in inflammation and angiogenesis. However, it is important to note that the transcriptional responses of specific leukocyte or endothelial cell populations were not assessed in the current study and it is unclear whether transcriptional changes resulting from β-catenin activation in myocytes influence inflammation and angiogenesis post-infarction. In addition, β-catenin was also found to modulate a number of genes related to cardiomyocyte metabolism in the adult heart. One such downregulated β-catenin responsive gene in the adult heart was *Ppargc1a,* which is a master regulator of mitochondrial biogenesis that governs the transition from a glycolytic to oxidative metabolic state in adult cardiomyocytes (Bhalla et al., 2014). Similarly, β-catenin also down regulated Nr4a3, which regulates the switch from glycolysis to oxidative phosphorylation metabolism and induces hypertrophy of skeletal muscle (Feng et al., 2015; Pearen et al., 2008). Furthermore, caBCAT induced the expression of a key lactate transporter called Slc16a3 in adult cardiomyocytes. It has previously been shown that *Slc16a3* is widely expressed in glycolytic skeletal muscle (Uhlén et al., 2015) and highly expressed in glycolytic proliferative adult cardiomyocytes *in vivo* (Honkoop et al., 2019). Therefore, these observations may indicate that β-catenin sustains contractile function after cardiac injury by enabling usage of alternative fuel sources (glucose and lactate) for adult cardiomyocyte energy production. Further studies will be required to pinpoint the precise molecules that mediate such effects. Nevertheless, this β-catenin-induced metabolic program is insufficient to drive adult cardiomyocyte proliferation.

This study demonstrates that β-catenin has distinct roles in immature and mature cardiomyocytes. β-catenin drives a cell cycle-related gene network and promotes proliferation of immature neonatal cardiomyocytes and hPSC-CMs. In contrast, β-catenin is redirected from mitotic genes to inflammatory, angiogenic and glycolytic metabolism-related gene targets in the adult heart, which is associated with cardioprotective effects post-MI. Thus, β-catenin may metabolically reprogram adult cardiomyocytes via induction of a neonatal-like glycolytic metabolic program. These findings suggest that Wnt/β-catenin drives distinct proliferative and metabolic networks in regenerative and non-regenerative cardiomyocytes, respectively, which may contribute towards the inability of the adult heart to regenerate following injury.

Materials and Methods

Ethical approval for animal experiments

Ethical approval for neonatal and adult mouse procedures was obtained from The University of Queensland's Animal Ethics Committee (AEC approval #SBMS/101/13/NHMRC or #SBMS/AIBN/138/16/NHMRC/NHF) or from the QIMR Berghofer Medical Research Institute Animal Ethics Committee (AEC approval #A18603M). All animal research was performed in accordance with National Health and Medical Research Council *Guidelines to Promote the Wellbeing of Animals Used for Scientific Purposes.*

Neonatal mouse AAV injections.

Timed pregnant CD1 (MGI:5649524) female mice were housed under standard conditions with 12-hour light/dark cycles and ad libitum access to food and water. At P1, neonatal CD-1 mice were separated from their mother and were anaesthetised by placing on ice for 1-2 minutes until the pups were motionless. The mice were then removed from ice, positioned laterally and a LED surgical lamp was used to transilluminate the superficial temporal vein. A Hamilton syringe with a 30-gauge needle was used to inject 20 µL of ether $1x10^{11}$ AAV6-caBCAT, $1x10^{11}$ AAV6-GFP or PBS into the superficial temporal vein. Viruses were diluted in PBS. Correct needle placement was verified by observing flushing of blood from the afferent segment of the vein. After viral injection, each pup was then rapidly warmed under a heat lamp until moving normally and returned to littermates. Once the entire litter had been injected, the pups were cleaned, rolled in mother's bedding and returned to the mother's cage. For mice pulsed with BrdU, the mice then received an injection of 5-bromo-2'-deoxyuridine (BrdU) (100 mg/kg, i.p.) on the day of viral injection and were subsequently injected with BrdU every 2nd day for 6 doses.

Neonatal mouse IWR-1 injections.

At P1, CD-1 pups were separated from mother and injected subcutaneously with either 40 µg of IWR-1 (~20 mg/kg) or 8 µL of DMSO. After each mouse was injected, the pups were, cleaned, rolled in the mother's bedding and returned to the mother simultaneously. Injections were continued daily until hearts were collected for analysis. For qPCR, neonatal mice

received injections at P1 and P2 and were collected at P2.5. For immunofluorescence, mice were injected daily until P7 and collected at P7.5.

Adult mouse intracardiac AAV injections and MI.

8-week-old adult CD-1 male mice were housed in standard conditions with ad libitum access to normal chow and water. The mice were anaesthetised in a stinger box with 2% isoflurane (Bayer), then intubated and ventilated with 0.25 L/min oxygen with a tidal volume of 250 µL and a respiration rate = 133 strokes/min (Minivent, Harvard Apparatus). Mice were positioned on a heated surgical mat to maintain body temperature. Once fully anaesthetised, the ventrolateral left chest was shaved, and a lateral thoracotomy was performed at the 4th intercostal space. The pericardium was separated using fine nosed tweezers. A 7-0 prolene suture was used to permanently ligate the left anterior descending coronary artery. MI was verified by observing blanching of the myocardium. A Hamilton syringe with a 30-gauge needle was used to inject 1x10^{11} AAV particles (i.e. caYAP, caBCAT or GFP control). Viruses were diluted in sterile PBS to a final injection volume of 20 µL for all injection groups; 4 separate injections of 5 µL were injected around the infarct penumbra. Following injection, the chest wall was closed using 4-0 silk suture and the overlying skin sutured with 6-0 prolene suture. The mice were supplied with a s.c. injection of buprenorphine (0.1 mg/kg) and carprofen (10 mg/kg) and allowed to recover. Starting from the day of the surgery, mice received BrdU injections (100 mg/kg, i.p.) every second day for 6 doses.

Adeno-associated virus construction

Sequences for caBCAT and caYAP were obtained from Addgene with the accessions 31787 and 42239, respectively. caBCAT was originally generated by deletion of the N-terminal 90 amino acids of human *CTNNB1* (Tward et al., 2007). caYAP contained a serine to alanine mutation of residue 127 of human *YAP1* (von Gise et al., 2012). caBCAT and caYAP were subcloned into pAAV-CDNA-V5His (Vector Biolabs) and encapsulated in AAV6 by Vector Biolabs. All constructs utilised a CMV promoter. AAV6-GFP was obtained from Vector Biolabs (Cat #7008).

Echocardiography.

Echocardiography for neonate i.v. AAV6-caBCAT and AAV6-GFP mice was performed on day 28 post injection. For adult MI experiments, echocardiography was performed on D0 (day of surgery), D3, D7, D21 and D28. Mice were anesthetized with 2% isoflurane (Bayer) with a flow rate of 0.25 L/min oxygen. The mice were then arranged supine on a heated mat. The ventrolateral left chest was shaved, and then pre-warmed ultrasound fluid was distributed on the chest. M-mode transverse images of the heart were then obtained using a HD15 Philips ultrasound machine. Fractional shortening and ejection fraction were calculated using HD15 software on measurements obtained from these images. The mice were then removed from isoflurane and monitored until they made a full recovery.

Isolation of adult cardiac cell populations for FACS and RNA-seq.

3 days after MI surgery, adult CD-1 mice were terminally anesthetized with an i.p injection of ketamine (100 mg/kg) and xylazine (12.5 mg/kg). The hearts were excised and washed in Perfusion Buffer (120.4 mM NaCl, 14.7 mM KCl, 0.6 mM KH2PO4, 0.6 mM Na2HPO4, 1.2 mM MgSO4•7H2O, 4.6 mM NaHCO3, 10 mM Na-HEPES, 30 mM taurine, 5.5 mM glucose and 10 mM 2,3-Butanedione 2-monoxime). A 21-gauge cannula was inserted into the aorta, taking care not to insert it through the aortic valve, and then secured with 3-0 silk suture. The cannulated hearts were suspended on a Langendorff apparatus and were retroperfused at a rate of 4 mL/min with oxygenated Perfusion Buffer at a temperature of 37˚C. Once extraneous tissue and atria were removed, digestion buffer (200 µg/ml Liberase DH (Roche) in perfusion buffer) was retroperfused through the heart for ~8 minutes. The hearts were cut into small pieces (1-2 mm^3) with fine scissors in Perfusion Buffer and then triturated with a 10 ml pipette. Heart cells were transferred through a 100 µm cell strainer and centrifuged at 30 x g for 3 minutes at room temperature. The non-myocyte enriched supernatant was used to isolate fibroblasts, leukocytes and endothelial cells using FACS. The myocyte pellet was washed with perfusion buffer, re-centrifuged and processed for RNA-seq.

FACS of non-myocyte cardiac cells.

FACS was performed as per a previously published protocol (Quaife-Ryan et al., 2017). Isolated non-myocyte cells were resuspended in 100 µl of 5% bovine serum albumin (BSA)/PBS solution (137 mM NaCl, 2.7 mM KCl, 1.8 mM KH2PO4, 10 mM Na2HPO4 and 75 µM bovine serum albumin) solution. The cells were then incubated at 4°C for 20 minutes with CD90-APC (1:33, A14727, ThermoFisher), CD45-FITC (1:10, 130-102-778, Miltenyi Biotec), CD31-BV421 (1:33, 102423, BioLegend) and Podoplanin-PE/Cy7 (1:66, 127411, BioLegned) in 100 µL 5% BSA/PBS. The cell isolates were washed in 5% BSA/PBS solution and sorted with a BD FACS ARIA cell sorter. The purified cell populations were centrifuged at 1000 x g for 5 minutes. The supernatant was removed and cell pellets were resuspended in 1 mL Trizol. See Table S1 for antibodies

hPSC-CM generation

Ethical approval for the use of human ESCs was obtained from The University of Queensland's Medical Research Ethics Committee (2014000801). All cell lines were tested for contamination and karyotypic abnormalities. Cardiomyocytes were produced using published protocols (Mills et al., 2019; Tiburcy et al., 2017; Voges et al., 2017). Briefly, cardiomyocyte/stromal cell cultures were produced from HES3 human embryonic stems cells (hESCs, WiCell) maintained using mTeSR-1 (Stem Cell Technologies). hESCs were seeded at $2x10^4$ cells/cm2 in Matrigel coated flasks and cultured for 4 days using mTeSR-1 and passaged with TrypLE (ThermoFisher). Subsequently, hESCs were differentiated into cardiac mesoderm by culturing for 3 days in RPMI B27- medium (RPMI 1640 GlutaMAX + 2% B27 supplement minus insulin (ThermoFisher), 200 µM L-ascorbic acid (Sigma), 1% Penicillin/Streptomycin (ThermoFisher)) and growth factors: 5 ng/ml BMP-4 (R&D Systems), 9 ng/ml Activin A (R&D Systems), 5 ng/ml FGF-2 (R&D Systems) and 1 µM CHIR99021 (STEMCELL Technologies, Cat # 72054). Media was exchanged daily. Cardiomyocyte specification was completed by 3 days of culture in RPMI B27- media with 5 µM IWP-4 (STEMCELL Technologies), followed by another 7 days of culture with RPMI B27+ (RPMI 1640 GlutaMAX + 2% B27 supplement with insulin (ThermoFisher), 200 µM L-ascorbic acid (Sigma) and 1% Penicillin/Streptomycin (ThermoFisher)). The cardiac cells, comprised of ~75% cardiomyocytes, ~25% CD90+ stromal cells (Voges et al., 2017) were dissociated at 15 days using human cardiac digestion buffer: 0.2% collagenase type I (Sigma) in 20% fetal bovine serum (FBS) in PBS (with Ca2+ and Mg2+) for 45 min at 37°C. The cardiac cells

were further digested with 0.25% trypsin-EDTA for 10 min. The cells were strained through a 100 µm filter, centrifuged at 300 x g for 3 min, and resuspended at the required density for 3D culture in CTRL Medium: α-MEM GlutaMAX (ThermoFisher), 10% FBS, 200 µM L-ascorbic acid (Sigma) and 1% Penicillin/Streptomycin (ThermoFisher).

Large hCO fabrication and culture.

For large hCO, cardiac cultures were differentiated for 15 days from either HES3 or HES3 NKX2-5$^{eGFP/w}$ (Elliott et al., 2011) cell lines and hCO were fabricated using published methods (Voges et al., 2017). For each hCO, 5 x 10^5 cardiac cells in CTRL medium were mixed with collagen I to make a 150 µL final solution containing 1 mg/ml collagen I. Collagen I was then salt-balanced with 10X DMEM (ThermoFisher) and pH neutralised with 0.1 M NaOH prior to mixing with Matrigel and cells. The mixture was prepared on ice and pipetted into circular PDMS moulds (Sylgard 184, Dow Corning). The collagen was allowed to gel at 37°C for 1 h prior to adding CTRL media to cover the tissues (~3 ml/hCO). hCO were cultured for 5 days in moulds, with media changes every 2 days. The hCO were transferred onto PDMS exercise poles and cultured for a further 7 days with media changes every 2-3 days. On day 27, hCO were treated with DMSO (Sigma) (0.15%), 5 µm CHIR99021 (Stem Cell Technologies), iCRT14 (50µM Concentration) (Tocris) or CHIR+iCRT14 and collected for analysis at 24 hrs or 48 hrs.

FACS of hPSC-CMs.

2D cardiac cells after 15 days of culture were treated with either 0.05% DMSO or 5 µM CHIR for 24 h before dissociation. For hCO, dissociation was performed using human cardiac digestion buffer for 45 min at 37°C, followed by 0.25% trypsin-EDTA for 10 min. The digested cells were then passed through a 100 µm mesh cell strainer (BD Biosciences), centrifuged at 300 x g for 3 min. Cells were incubated with primary antibodies (see Table S1) for 15 min at 4°C in FACS buffer (5% FBS in PBS), washed and then incubated with secondary fluorophore antibodies (see Table S1) in FACS buffer for 15 min at 4°C. The cells were then washed and re-suspended in PBS for FACS. Live cells were gated on forward- and side-scatter, doublets were excluded based on forward- and side-scatter width and height. CD90+ cells and CD90- cells from human cardiac cultures were previously demonstrated to be stromal cells and cardiomyocytes, respectively (Voges et al., 2017).

RNA isolation, cDNA generation and qPCR

RNA was isolated from tissues or cells using TRIzol® (ThermoFisher Scientific) as per manufacturer's instructions, unless otherwise specified. For whole tissues, tissues were homogenised in 1 mL of TRIzol and left at room temperature for 3 minutes to fully dissociate nucleoprotein complexes. 200 µL of chloroform was added, samples were vortexed for 30 seconds, incubated for 3 minutes at room temperature and centrifuged at 12,000 x g for 15 minutes at 4°C. The aqueous phase containing RNA was transferred to a new Eppendorf tube, 1 mL of isopropanol was added and 1 µL of GlycoBlue™ (ThermoFisher) was used as a precipitant. The RNA pellet was washed in 75% ethanol/ 25% nuclease free water, allowed to dry and then resuspended in 87.5 µL nuclease-free water and incubated at 55°C for 15 minutes.

For cDNA generation, RNA was first treated with RNase-free DNase (QIAGEN) and then column-isolated using RNeasy MinElute Clean-up kit (QIAGEN) as per manufacturer's instructions. RNA was eluted from MinElute columns with 20 µL of nuclease-free water. RNA was then used for qPCR or RNA-seq

Superscript III first-strand synthesis system (Invitrogen) was used to generate cDNA. DNase-treated RNA was prehybridised with 1 µL 150 ng random hexamer primers and 1 µL 10 mM dNTPs at 65°C for 5 minutes and placed on ice. The SuperScript® reaction mix was added (4 µL of 5x First strand buffer, 1 µL of 0.1 mM dithiothreitol and 1 µL of RNase OUT (ThermoFisher) and 1 µL of SuperScript® III (ThermoFisher). Reverse transcriptase free controls had all the same reagents but without SuperScript® III. cDNA was generated using a thermocycler at 25 °C for 10 minutes, 50 °C for 60 minutes and 70 °C for 15 minutes.

qPCR was performed using SYBR™ Green PCR Master Mix (ThermoFisher) or PowerUp™ SYBR™ Green (ThermoFisher) as per manufacturer's recommendations. Primers were designed using NCBI Primer-BLAST (Ye et al., 2012) with the following parameters: PCR product size >80 and <150 bp, Tm = ~59°C, if possible primer spans exon-exon junctions and target specificity assessed against Refseq mRNA database. qPCR was performed with a QuantStudio™ 5 system (Applied Biosystems) using manufacturer's instructions. Endogenous controls for mouse and human were either 18S ribosomal RNA (*18s*) or hypoxanthine-guanine phosphoribosyltransferase (*Hprt or HPRT1*) as specified. Primer sequences for qPCR are listed in Table S22.

ChIP-seq of hPSC-CMs.

2D hPSC-CM were treated for 24 hours with 5 µm CHIR. hPSC-CMs were fixed for 10 minutes at room temperature with 1% paraformaldehyde (PFA) in CTRL medium. Cross-linking was stopped by addition 0.125M glycine for 5 minutes. Cells were washed 2x with ice cold PBS and then scraped in 1mL PBS into a 1.5mL Eppendorf tube. Fixed cells were spun (200xg, 10 minutes) and treated with lysis buffer according to the MAGnify Chromatin Immunoprecipitation kit protocol (150 µL/3 million cells assuming 15x106 cells/flask). Chromatin was sheared using a Bioruptor UCD2000 sonicator with the following settings: 12x cycles of 30 seconds sonication with 90 seconds cooling. Chromatin was sonicated in 1.5 mL eppendorf tubes, and the volume of cell lysate in each tube during sonication was kept at 150 µL. Sheared chromatin in lysis buffer was stored at -80°C prior to ChIP. ChIP reactions were carried out with MAGnify Chromatin Immunoprecipitation System (ThermoFisher) reagents as per manufacturer's instructions. Antibodies used in ChIP reactions were: 1 µg anti-TCF4 (Santa Cruz: sc-8631 X), 3 µL anti-H3K4me3 (Active Motif; 39159), 5 µg anti-H3K27ac (Active Motif; 39133). ChIP-seq Libraries were created with TruSeq ChIP Library Preparation Kit (Illumina) with DNA size selected and quality controlled by Pippin Prep size selection (Sage Science). Libraries were read with HiSeq SR Cluster v4 kit (Illumina) on a HiSeq 2500 sequencer with 50-bp single-end reads. Quality control data are summarized Table S3.

RNA-seq of 2D CHIR treated 2D hPSC-CM and CD90+ stromal cells

Libraries were constructed with Ovation RNA-Seq system V2 (for SPIA amplifications and cDNA generation) coupled with the Ovation Ultralow System (NuGEN). 7 rounds of amplification were performed. The quality of libraries was ascertained with Qubit. Libraries were read with 50bp SR Rapid Mode on a HiSeq1500 (Illumina).

RNA-seq of isolated adult AAV-BCAT and AAV-GFP cardiomyocytes

Once purified RNA was obtained, ribosomal RNA was depleted with Ribo Zero Gold (Illumina), RNA quality was verified utilising MultiNA bioanalyzer (Shimadzu), and cDNA generated with SuperScript II Reverse Transcriptase (ThermoFisher). RNA-seq libraries were generated with TruSeq Stranded Total RNA kits (Illumina) and read with HiSeq SR

Cluster v4 kit (Illumina) on a HiSeq 4000 sequencer (Illumina). RNA-seq mapping quality control data are listed in Table S4.

Cellularisation of fixed hearts for cardiomyocyte cell counting

Cardiomyocytes were isolated 28 days after P1 i.v AAV injection, as per a previously published protocol (Bywater et al., 2020). Hearts were isolated from P1.d28 mice, washed with PBS and fixed in 1% PFA overnight at 4°C. The next day, the hearts were washed 4 times in PBS. The atria were removed and the ventricles were diced into 1-2 mm^3 pieces and incubated with 0.5 U/mL collagenase B (Roche #11088807001) in 0.2% NaN_3/PBS and oscillated (1000 rpm) at 37 °C. The supernatant containing cardiomyocytes were collected every 12 hours and kept at 4 °C in 0.2% NaN3/FBS. Once dissociation was complete, the cardiomyocytes were centrifuged at 1000xg for 3 minutes, washed twice in PBS and stored in 0.2% NaN3/PBS at 4°C. The cardiomyocytes were then counted on a haemocytometer.

Histology

Unless otherwise specified, animals were euthanised and tissues were briefly wash in PBS and then fixed in 4% paraformaldehyde/PBS on a shaker overnight. The tissues were then washed in PBS and then processed for paraffin embedded sectioning. Fixed heart tissues were cut transversely, dehydrated in sequential graduated ethanol washes, washed twice in xylene and embedded in paraffin wax cassettes. Tissues were then sectioned at 6 µm and mounted on SuperFrost Ultra Plus™ slides (FisherScientific). For Masson's Trichrome staining, sections were deparaffinized and rehydrated in ethanol, washed in distilled water, stained in Weigert's iron haematoxylin for 10 minutes and washed in distilled water for 10 minutes. Sections were then stained in Biebrich scarlet-acid fuchsin solution for 10 minutes and further washed in distilled water. Fibrotic tissue was differentiated in phosphomolybdic-phosphotungstic acid solution for 10 minutes and directly transferred to aniline blue solution for 0.5-3 minutes (depending on the strength of aniline blue dye). The sections were washed in distilled water until the water ran clear and then further differentiated in 1% acetic acid/distilled water solution for 3 minutes. Sections were washed in distilled water, dehydrated in sequential graduated ethanol washes, cleared with xylene and then mounted with DPX mounting media (Sigma).

Whole-Mount Immunostaining of hCOs.

hCOs were fixed with 1% paraformaldyhyde/PBS solution for 60 minutes at room temperature. The hCOs with PBS 3 times and stained with primary antibodies (Table S1) in Blocking Buffer, 5% FBS, and 0.2% Triton X-100 (Sigma) in PBS overnight at 4 °C. Cells were then washed in Blocking Buffer two times for 2 h and subsequently incubated with secondary antibodies (Table S1) and Hoescht (1:1,000) overnight at 4 °C. They were washed in Blocking Buffer two times for 2 h and imaged in situ or mounted on microscope slides using Fluoromount-G (Southern Biotech).

Immunofluorescent staining of mouse heart sections

Hearts were fixed in 4% PFA in PBS overnight, washed in PBS and halved with a single transverse cut at the ligature mark or for non-infarcted mice, equidistant from base and apex. The hearts were dehydrated and embedded in paraffin wax. Each sample was sectioned at 6 µm. Sections were rehydrated, blocked with 10% goat serum in PBS and stained with primary antibodies (See Table S1) in 2% goat serum/PBS overnight at 4°C. Sections were then washed with PBS stained with secondary antibodies and Hoechst 33342 (Life Technologies) diluted 1:1000 in 2% goat serum/PBS for 1 hour at room temperature and mounted in FluoMount® (ThermoFisher). Each slide was then imaged using a Leica DMi8 confocal microscope. For adult cardiomyocyte proliferation analysis, 4 cross sections for each heart were quantified. The number of positively stained cardiomyocytes were normalised per section. Each section was separated by 250 µm. For neonatal proliferation analysis, 10 images from 2 sections from each heart were quantified. The number of positive cardiomyocytes were normalised to the total number of cardiomyocytes in each image.

Bioinformatics for RNA-seq analysis

Poor quality sequence (<30 phred score) and adapters were clipped using Trimmomatic (v 0.36.6) (Bolger et al., 2014). Reads were mapped to either the human or mouse GRCh38/hg38 reference genome using STAR (v2.4.0g1) (Dobin et al., 2013) . HTSeq-count (Anders et al., 2015) on union mode was used to generate count matrices. Differential expression analysis was performed with EdgeR(v3.2.4) (Robinson et al., 2010). For CHIR RNA-seq, differential analysis was performed with the EdgeR command glmLRT [log2(fold change) set to > 1 or < -1, FDR < 0.05]. For adult mouse MI myocyte RNA-seq, differential

analysis was performed with the EdgeR command glmLRT [FDR < 0.1]. Gene ontological analysis was performed using DAVID (Huang et al., 2007). Principal coordinate analysis was performed with the plotMDS function in EdgeR. Heatmaps were assembled GENE-E (Broad Institute). See Table S5 for all bioinformatic tools used in this study

Bioinformatics for hPSC-CM ChIP-seq analysis

Trimmomatic (v 0.36.6) (Bolger et al., 2014) was used to trim adapter and poor quality sequences (<20 phred score). Reads were then mapped with Bowtie2 (v 2.3.4.1) (Langmead and Salzberg, 2012) to the reference human genome sequence GRCh37/hg19. Peaks were called with the callpeak function of MACS2 (v 2.1.1.0) (Zhang et al., 2008) with default parameters (q-value < 0.01). For histone marks, broadpeaks were called using broad subcommand with --broad.cutoff= 0.1. Replicate peaks were intersected using the intersect function of GenomicRanges (v1.34.0) (Lawrence et al., 2013). All ChIP-seq heatmaps and correlations were generated with deepTools2 (v 2.5.1.1.0) (Ramírez et al., 2016). Gene ontological analysis of ChIP-seq peaks was performed by associating closest known transcription start sites with GREAT (v3.0.0) (McLean et al., 2010). Motif binding site analyses were performed with findMotifsGenome function in Homer (v4.10)(Heinz et al., 2010). See Table S5 for all bioinformatic tools used in this study

Bioinformatic comparison of human and mouse RNA-seq and ChIP-seq datasets.
Ensembl IDs for orthologous genes between human and mouse were obtained using the biomaRt (v 2.38.0) (Durinck et al., 2009) package in R. Venn diagrams were then used to identified co-regulated genes between the datasets.

Other RNA-seq datasets utilised in analysis

Data used in some comparative analyses were obtained from Quaife-Ryan, et al., 2017 or Mills, et al., 2017 as indicated. The “neonatal regenerative gene network” used in these analyses was obtained from Quaife-Ryan, et al., 2017 (GSE95755). We previously demonstrated that adult cardiomyocytes and endothelial cells do not reactivate a neonatal proliferative program following myocardial infarction (Quaife-Ryan et al., 2017). The “neonatal regenerative gene network” used in Fig. 6 contains genes that were highly expressed in neonatal regenerating cardiac cells but were not deployed by adult cardiomyocytes and endothelial cells following MI. This gene network was replete with cell-

cycle genes and was bioinformatically predicted to drive proliferative responses in the regenerating heart (Quaife-Ryan et al., 2017). We subsequently demonstrated that induction of c-Myc/pTEFb transcription reactivated this neonatal regenerative gene network in adult cardiomyocytes (Bywater et al., 2020). Original datasets are available at the Gene Expression Omnibus using accessions GSE93841 (human fetal and adult heart RNA-seq),GSE95755 (mouse regenerative gene network RNA-seq), and GSE95764 (cardiomyocyte nuclei RNA-seq and ATAC-seq).

Non-bioinformatic statistical analysis

An unpaired two-tailed student's t-test was used for comparisons between two groups. For comparison of more than 2 groups, a one-way ANOVA followed by a Tukey's multiple comparisons post-test was used. A two-way ANOVA with a Tukey post-test was used to test multiple groups with 2 or more independent variables. In all figures, * = $p < 0.05$, ** = $p < 0.01$, *** = $p < 0.001$ and **** = $p < 0.0001$. All data are represented as ± SEM unless otherwise specified. Further statistical analysis information is presented in the figure legends. For mouse studies, n represents the number of mice. For human PSC-derived cardiac cell experiments, n represents individual experiments.

Acknowledgments

We thank V. Nink and G. Osbourne for their assistance with FACS at the Flow Cytometry facility at the Queensland Brain Institute, QFAB bioinformatics and I. Makunin at Galaxy Australia (https://usegalaxy.org.au/) for bioinformatics training, the Developmental Studies Hybridoma Bank for antibodies and the Monash Health Translational Precinct Medical Genomics Facility and Australian Genome Research Facility for sequencing. We also thank A. Masel and C. Winterford at the QIMR Berghofer histology facility for assistance with immunostaining. Some of the data in this paper forms part of the lead author's (G.A.Q.-R.) PhD thesis, which was published online in 2020 by The University of Queensland (DOI: 10.14264/uql.2020.927).

Competing Interests

G.A.Q.-R., R.J.M., J.E.H., and E.R.P. are co-inventors on patents for hCO maturation and cardiac regeneration held by The University of Queensland and QIMR Berghofer Medical Research Institute. J.E.H. is a co-inventor on licensed patents held by the University of Goettingen. R.J.M, E.R.P. and J.E.H. are co-founders, scientific advisors and stockholders in Dynomics.

Funding

J.E.H. and E.R.P. acknowledge grant and fellowship support from the National Health and Medical Research Council of Australia, the Heart Foundation of Australia, the Stafford Fox Medical Research Foundation, Stem Cells Australia and QIMR Berghofer Medical Research Institute. The Murdoch Children's Research Institute is supported by the Victorian Government's Operational Infrastructure Support Program.

Data Availability

The CHIR hPSC-CM RNA-seq, adult mouse caBCAT RNAseq and TCF7L2 ChIP-seq datasets are all available at the Gene Expression Omnibus under the accession GSE150521 (https://www.ncbi.nlm.nih.gov/geo/).

References

Alkass, K., Panula, J., Westman, M., Wu, T.-D., Guerquin-Kern, J.-L. and Bergmann, O. (2015). No Evidence for Cardiomyocyte Number Expansion in Preadolescent Mice. *Cell* **163**, 1026-1036.

Anders, S., Pyl, P. T. and Huber, W. (2015). HTSeq--a Python framework to work with high-throughput sequencing data. *Bioinformatics* **31**, 166-169.

Arany, Z., He, H., Lin, J., Hoyer, K., Handschin, C., Toka, O., Ahmad, F., Matsui, T., Chin, S., Wu, P.-H., et al. (2005). Transcriptional coactivator PGC-1 alpha controls the energy state and contractile function of cardiac muscle. *Cell metabolism* **1**, 259-271.

Aurora, A. B., Porrello, E. R., Tan, W., Mahmoud, A. I., Hill, J. A., Bassel-Duby, R., Sadek, H. A. and Olson, E. N. (2014). Macrophages are required for neonatal heart regeneration. *Journal of Clinical Investigation*.

Bassat, E., Mutlak, Y. E., Genzelinakh, A., Shadrin, I. Y., Baruch-Umansky, K., Yifa, O., Kain, D., Rajchman, D., Leach, J., Bassat, D. R., et al. (2017). The extracellular matrix protein Agrin promotes heart regeneration in mice. *Nature* **271**, H2183.

Bergmann, O., Zdunek, S., Felker, A., Salehpour, M., Alkass, K., Bernard, S., Sjostrom, S. L., Szewczykowska, M., Jackowska, T., Dos Remedios, C., et al. (2015). Dynamics of Cell Generation and Turnover in the Human Heart. *Cell* **161**, 1566-1575.

Bhalla, K., Liu, W.-J., Thompson, K., Anders, L., Devarakonda, S., Dewi, R., Buckley, S., Hwang, B.-J., Polster, B., Dorsey, S. G., et al. (2014). Cyclin D1 represses gluconeogenesis via inhibition of the transcriptional coactivator PGC1α. *Diabetes* **63**, 3266-3278.

Bolger, A. M., Lohse, M. and Usadel, B. (2014). Trimmomatic: a flexible trimmer for Illumina sequence data. *Bioinformatics* **30**, 2114-2120.

Bywater, M. J., Burkhart, D. L., Straube, J., Sabò, A., Pendino, V., Hudson, J. E., Quaife-Ryan, G. A., Porrello, E. R., Rae, J., Parton, R. G., et al. (2020). Reactivation of Myc transcription in the mouse heart unlocks its proliferative capacity. *Nature Communications* **11**, 1827.

Chen, B., Dodge, M. E., Tang, W., Lu, J., Ma, Z., Fan, C.-W., Wei, S., Hao, W., Kilgore, J., Williams, N. S., et al. (2009). Small molecule-mediated disruption of Wnt-dependent signaling in tissue regeneration and cancer. *Nature chemical biology* **5**, 100-107.

Chen, X., Shevtsov, S. P., Hsich, E., Cui, L., Haq, S., Aronovitz, M., Kerkelä, R., Molkentin, J. D., Liao, R., Salomon, R. N., et al. (2006). The beta-catenin/T-cell factor/lymphocyte enhancer factor signaling pathway is required for normal and stress-induced cardiac hypertrophy. *Molecular and cellular biology* **26**, 4462-4473.

D'Uva, G., Aharonov, A., Lauriola, M., Kain, D., Yahalom-Ronen, Y., Carvalho, S., Weisinger, K., Bassat, E., Rajchman, D., Yifa, O., et al. (2015). ERBB2 triggers mammalian heart regeneration by promoting cardiomyocyte dedifferentiation and proliferation. *Nature cell biology* **17**, 627-638.

Dobin, A., Davis, C. A., Schlesinger, F., Drenkow, J., Zaleski, C., Jha, S., Batut, P., Chaisson, M. and Gingeras, T. R. (2013). STAR: ultrafast universal RNA-seq aligner. *Bioinformatics* **29**, 15-21.

Duan, J., Gherghe, C., Liu, D., Hamlett, E., Srikantha, L., Rodgers, L., Regan, J. N., Rojas, M., Willis, M., Leask, A., et al. (2012). Wnt1/βcatenin injury response activates the epicardium and cardiac fibroblasts to promote cardiac repair. *The EMBO journal* **31**, 429-442.

Durinck, S., Spellman, P. T., Birney, E. and Huber, W. (2009). Mapping identifiers for the integration of genomic datasets with the R/Bioconductor package biomaRt. *Nature Protocols* **4**, 1184-1191.

Elliott, D. A., Braam, S. R., Koutsis, K., Ng, E. S., Jenny, R., Lagerqvist, E. L., Biben, C., Hatzistavrou, T., Hirst, C. E., Yu, Q. C., et al. (2011). NKX2-5(eGFP/w) hESCs for isolation of human cardiac progenitors and cardiomyocytes. *Nature Methods* **8**, 1037-1040.

Eulalio, A., Mano, M., Dal Ferro, M., Zentilin, L., Sinagra, G., Zacchigna, S. and Giacca, M. (2012). Functional screening identifies miRNAs inducing cardiac regeneration. *Nature* **492**, 376-381.

Feng, X.-J., Gao, H., Gao, S., Li, Z., Li, H., Lu, J., Wang, J.-J., Huang, X.-Y., Liu, M., Zou, J., et al. (2015). The orphan receptor NOR1 participates in isoprenaline-induced cardiac hypertrophy by regulating PARP-1. *British journal of pharmacology* **172**, 2852-2863.

Gilsbach, R., Schwaderer, M., Preissl, S., Grüning, B. A., Kranzhöfer, D., Schneider, P., Nührenberg, T. G., Mulero-Navarro, S., Weichenhan, D., Braun, C., et al. (2018). Distinct epigenetic programs regulate cardiac myocyte development and disease in the human heart in vivo. *Nature communications*, 1-14.

Gonsalves, F. C., Klein, K., Carson, B. B., Katz, S., Ekas, L. A., Evans, S., Nagourney, R., Cardozo, T., Brown, A. M. and DasGupta, R. (2011). An RNAi-based chemical genetic screen identifies three small-molecule inhibitors of the Wnt/wingless signaling pathway. *Proc Natl Acad Sci U S A* **108**, 5954-5963.

Hahn, J.-Y., Cho, H.-J., Bae, J.-W., Yuk, H.-S., Kim, K.-I., Park, K.-W., Koo, B.-K., Chae, I.-H., Shin, C.-S., Oh, B.-H., et al. (2006). Beta-catenin overexpression reduces myocardial infarct size through differential effects on cardiomyocytes and cardiac fibroblasts. *The Journal of biological chemistry* **281**, 30979-30989.

Heallen, T., Zhang, M., Wang, J., Bonilla-Claudio, M., Klysik, E., Johnson, R. L. and Martin, J. F. (2011). Hippo Pathway Inhibits Wnt Signaling to Restrain Cardiomyocyte Proliferation and Heart Size. *Science (New York, N.Y.)* **332**, 458-461.

Heinz, S., Benner, C., Spann, N., Bertolino, E., Lin, Y. C., Laslo, P., Cheng, J. X., Murre, C., Singh, H. and Glass, C. K. (2010). Simple combinations of lineage-determining transcription factors prime cis-regulatory elements required for macrophage and B cell identities. *Molecular Cell* **38**, 576-589.

Hirose, K., Payumo, A. Y., Cutie, S., Hoang, A., Zhang, H., Guyot, R., Lunn, D., Bigley, R. B., Yu, H., Wang, J., et al. (2019). Evidence for hormonal control of heart regenerative capacity during endothermy acquisition. *Science (New York, N.Y.)* **364**, 184-188.

Honkoop, H., de Bakker, D. E., Aharonov, A., Kruse, F., Shakked, A., Nguyen, P. D., de Heus, C., Garric, L., Muraro, M. J., Shoffner, A., et al. (2019). Single-cell analysis uncovers that metabolic reprogramming by ErbB2 signaling is essential for cardiomyocyte proliferation in the regenerating heart. *eLife* **8**.

Hou, N., Ye, B., Li, X., Margulies, K. B., Xu, H., Wang, X. and Li, F. (2016). Transcription Factor 7-like 2 Mediates Canonical Wnt/β-Catenin Signaling and c-Myc Upregulation in Heart Failure. *Circulation. Heart failure* **9**.

Huang, D. W., Sherman, B. T., Tan, Q., Collins, J. R., Alvord, W. G., Roayaei, J., Stephens, R., Baseler, M. W., Lane, H. C. and Lempicki, R. A. (2007). The DAVID Gene Functional Classification Tool: a novel biological module-centric algorithm to functionally analyze large gene lists. *Genome biology* **8**, R183-116.

Iyer, L. M., Nagarajan, S., Woelfer, M., Schoger, E., Khadjeh, S., Zafiriou, M. P., Kari, V., Herting, J., Pang, S. T., Weber, T., et al. (2018). A context-specific cardiac β-catenin and GATA4 interaction influences TCF7L2 occupancy and remodels chromatin driving disease progression in the adult heart. *Nucleic acids research* **136**, 3205.

Langmead, B. and Salzberg, S. L. (2012). Fast gapped-read alignment with Bowtie 2. *Nature Methods* **9**, 357-359.

Lawrence, M., Huber, W., Pagès, H., Aboyoun, P., Carlson, M., Gentleman, R., Morgan, M. T. and Carey, V. J. (2013). Software for computing and annotating genomic ranges. *PLoS computational biology* **9**, e1003118.

Li, Z., Nie, F., Wang, S. and Li, L. (2011). Histone H4 Lys 20 monomethylation by histone methylase SET8 mediates Wnt target gene activation. *Proceedings of the National Academy of Sciences* **108**, 3116-3123.

Lin, Z., von Gise, A., Zhou, P., Gu, F., Ma, Q., Jiang, J., Yau, A. L., Buck, J. N., Gouin, K. A., van Gorp, P. R. R., et al. (2014). Cardiac-specific YAP activation improves cardiac function and survival in an experimental murine MI model. *Circulation Research* **115**, 354-363.

Magadum, A., Ding, Y., He, L., Kim, T., Vasudevarao, M. D., Long, Q., Yang, K., Wickramasinghe, N., Renikunta, H. V., Dubois, N., et al. (2017). Live cell

screening platform identifies PPARδ as a regulator of cardiomyocyte proliferation and cardiac repair. *Cell Research* **27**, 1002-1019.

Mahmoud, A. I., Kocabas, F., Muralidhar, S. A., Kimura, W., Koura, A. S., Thet, S., Porrello, E. R. and Sadek, H. A. (2013). Meis1 regulates postnatal cardiomyocyte cell cycle arrest. *Nature*.

Mahmoud, A. I., O'Meara, C. C., Gemberling, M., Zhao, L., Bryant, D. M., Zheng, R., Gannon, J. B., Cai, L., Choi, W.-Y., Egnaczyk, G. F., et al. (2015). Nerves Regulate Cardiomyocyte Proliferation and Heart Regeneration. *Developmental cell* **34**, 387-399.

McLean, C. Y., Bristor, D., Hiller, M., Clarke, S. L., Schaar, B. T., Lowe, C. B., Wenger, A. M. and Bejerano, G. (2010). GREAT improves functional interpretation of cis-regulatory regions. *Nature Biotechnology* **28**, 495-501.

Mills, R. J., Parker, B. L., Quaife-Ryan, G. A., Voges, H. K., Needham, E. J., Bornot, A., Ding, M., Andersson, H., Polla, M., Elliott, D. A., et al. (2019). Drug Screening in Human PSC-Cardiac Organoids Identifies Pro-proliferative Compounds Acting via the Mevalonate Pathway. *Cell Stem Cell* **24**, 895-907.e896.

Mills, R. J., Titmarsh, D. M., Koenig, X., Parker, B. L., Ryall, J. G., Quaife-Ryan, G. A., Voges, H. K., Hodson, M. P., Ferguson, C., Drowley, L., et al. (2017). Functional screening in human cardiac organoids reveals a metabolic mechanism for cardiomyocyte cell cycle arrest. *Proceedings of the National Academy of Sciences* **114**, E8372-E8381.

Mohamed, T. M. A., Ang, Y.-S., Radzinsky, E., Zhou, P., Huang, Y., Elfenbein, A., Foley, A., Magnitsky, S. and Srivastava, D. (2018). Regulation of Cell Cycle to Stimulate Adult Cardiomyocyte Proliferation and Cardiac Regeneration. *Cell* **173**, 104-116.e112.

Nakada, Y., Canseco, D. C., Thet, S., Abdisalaam, S., Asaithamby, A., Santos, C. X., Shah, A. M., Zhang, H., Faber, J. E., Kinter, M. T., et al. (2017). Hypoxia induces heart regeneration in adult mice. *Nature* **541**, 222-227.

Natarajan, N., Abbas, Y., Bryant, D. M., González-Rosa, J. M., Sharpe, M., Uygur, A., Cocco-Delgado, L. H., Ho, N. N., Gerard, N. P., Gerard, C. J., et al. (2018).

Complement Receptor C5aR1 Plays an Evolutionarily Conserved Role in Successful Cardiac Regeneration. *Circulation*, CIRCULATIONAHA.117.030801.

Noack, C., Zafiriou, M. P., Schaeffer, H. J., Renger, A., Pavlova, E., Dietz, R., Zimmermann, W. H., Bergmann, M. W. and Zelarayan, L. C. (2012). Krueppel-like factor 15 regulates Wnt/beta-catenin transcription and controls cardiac progenitor cell fate in the postnatal heart. *EMBO Mol Med* **4**, 992-1007.

Oerlemans, M. I. F. J., Goumans, M.-J., van Middelaar, B., Clevers, H., Doevendans, P. A. and Sluijter, J. P. G. (2010). Active Wnt signaling in response to cardiac injury. *Basic research in cardiology* **105**, 631-641.

Pearen, M. A., Myers, S. A., Raichur, S., Ryall, J. G., Lynch, G. S. and Muscat, G. E. O. (2008). The orphan nuclear receptor, NOR-1, a target of beta-adrenergic signaling, regulates gene expression that controls oxidative metabolism in skeletal muscle. *Endocrinology* **149**, 2853-2865.

Porrello, E. R., Mahmoud, A. I., Simpson, E., Hill, J. A., Richardson, J. A., Olson, E. N. and Sadek, H. A. (2011). Transient regenerative potential of the neonatal mouse heart. *Science (New York, N.Y.)* **331**, 1078-1080.

Porrello, E. R., Mahmoud, A. I., Simpson, E., Johnson, B. A., Grinsfelder, D., Canseco, D., Mammen, P. P., Rothermel, B. A., Olson, E. N. and Sadek, H. A. (2013). Regulation of neonatal and adult mammalian heart regeneration by the miR-15 family. *Proceedings of the National Academy of Sciences* **110**, 187-192.

Quaife-Ryan, G. A., Sim, C. B., Porrello, E. R. and Hudson, J. E. (2016). Resetting the epigenome for heart regeneration. *Seminars in cell & developmental biology* **58**, 2-13.

Quaife-Ryan, G. A., Sim, C. B., Ziemann, M., Kaspi, A., Rafehi, H., Ramialison, M., El-Osta, A., Hudson, J. E. and Porrello, E. R. (2017). Multicellular Transcriptional Analysis of Mammalian Heart Regeneration. *Circulation* **136**, 1123-1139.

Ramírez, F., Ryan, D. P., Grüning, B., Bhardwaj, V., Kilpert, F., Richter, A. S., Heyne, S., Dündar, F. and Manke, T. (2016). deepTools2: a next generation web server for deep-sequencing data analysis. *Nucleic acids research* **44**, W160-165.

Robinson, M. D., McCarthy, D. J. and Smyth, G. K. (2010). edgeR: a Bioconductor package for differential expression analysis of digital gene expression data. *Bioinformatics* **26**, 139-140.

Rumyantsev, P. P. and Borisov, A. (1987). DNA synthesis in myocytes from different myocardial compartments of young rats in norm, after experimental infarction and in vitro. *Biomedica biochimica acta* **46**, S610-615.

Sdek, P., Zhao, P., Wang, Y., Huang, C.-J., Ko, C. Y., Butler, P. C., Weiss, J. N. and MacLellan, W. R. (2011). Rb and p130 control cell cycle gene silencing to maintain the postmitotic phenotype in cardiac myocytes. *The Journal of cell biology* **194**, 407-423.

Soonpaa, M. H., Kim, K. K., Pajak, L., Franklin, M. and Field, L. J. (1996). Cardiomyocyte DNA synthesis and binucleation during murine development. *The American journal of physiology* **271**, H2183-2189.

Taegtmeyer, H., Sen, S. and Vela, D. (2010). Return to the fetal gene program: a suggested metabolic link to gene expression in the heart. *Annals of the New York Academy of Sciences* **1188**, 191-198.

Tiburcy, M., Hudson, J. E., Balfanz, P., Schlick, S., Meyer, T., Chang Liao, M.-L., Levent, E., Raad, F., Zeidler, S., Wingender, E., et al. (2017). Defined Engineered Human Myocardium With Advanced Maturation for Applications in Heart Failure Modeling and Repair. *Circulation* **135**, 1832-1847.

Tward, A. D., Jones, K. D., Yant, S., Cheung, S. T., Fan, S. T., Chen, X., Kay, M. A., Wang, R. and Bishop, J. M. (2007). Distinct pathways of genomic progression to benign and malignant tumors of the liver. *Proc Natl Acad Sci U S A* **104**, 14771-14776.

Uhlén, M., Fagerberg, L., Hallström, B. M., Lindskog, C., Oksvold, P., Mardinoglu, A., Sivertsson, Å., Kampf, C., Sjöstedt, E., Asplund, A., et al. (2015). Tissue-based map of the human proteome. *Science* **347**, 1260419.

Voges, H. K., Mills, R. J., Elliott, D. A., Parton, R. G., Porrello, E. R. and Hudson, J. E. (2017). Development of a human cardiac organoid injury model reveals innate regenerative potential. *Development (Cambridge, England)* **144**, 1118-1127.

von Gise, A., Lin, Z., Schlegelmilch, K., Honor, L. B., Pan, G. M., Buck, J. N., Ma, Q., Ishiwata, T., Zhou, B., Camargo, F. D., et al. (2012). YAP1, the nuclear target of Hippo signaling, stimulates heart growth through cardiomyocyte proliferation but not hypertrophy. *Proceedings of the National Academy of Sciences* **109**, 2394-2399.

Wang, S., Ye, L., Li, M., Liu, J., Jiang, C., Hong, H., Zhu, H. and Sun, Y. (2016). GSK-3β Inhibitor CHIR-99021 Promotes Proliferation Through Upregulating β-Catenin in Neonatal Atrial Human Cardiomyocytes. *Journal of cardiovascular pharmacology* **68**, 425-432.

Wang, W., Hu, C.-K., Zeng, A., Alegre, D., Hu, D., Gotting, K., Ortega Granillo, A., Wang, Y., Robb, S., Schnittker, R., et al. (2020). Changes in regeneration-responsive enhancers shape regenerative capacities in vertebrates. *Science* **369**, eaaz3090.

Wöhrle, S., Wallmen, B. and Hecht, A. (2007). Differential control of Wnt target genes involves epigenetic mechanisms and selective promoter occupancy by T-cell factors. *Molecular and cellular biology* **27**, 8164-8177.

Xin, M., Kim, Y., Sutherland, L. B., Qi, X., McAnally, J., Schwartz, R. J., Richardson, J. A., Bassel-Duby, R. and Olson, E. N. (2011). Regulation of insulin-like growth factor signaling by Yap governs cardiomyocyte proliferation and embryonic heart size. *Science Signaling* **4**, ra70-ra70.

Ye, J., Coulouris, G., Zaretskaya, I., Cutcutache, I., Rozen, S. and Madden, T. L. (2012). Primer-BLAST: A tool to design target-specific primers for polymerase chain reaction. *BMC Bioinformatics* **13**, 134.

Ye, L., D'Agostino, G., Loo, S. J., Wang, C. X., Su, L. P., Tan, S. H., Tee, G. Z., Pua, C. J., Pena, E. M., Cheng, R. B., et al. (2018). Early Regenerative Capacity in the Porcine Heart. *Circulation* **138**, 2798-2808.

Zhang, Y., Liu, T., Meyer, C. A., Eeckhoute, J., Johnson, D. S., Bernstein, B. E., Nusbaum, C., Myers, R. M., Brown, M., Li, W., et al. (2008). Model-based analysis of ChIP-Seq (MACS). *Genome biology* **9**, R137.

Zhao, X., Hua, Y., Chen, H., Yang, H., Zhang, T., Huang, G., Fan, H., Tan, Z., Huang, X., Liu, B., et al. (2015). Aldehyde dehydrogenase-2 protects against myocardial infarction-related cardiac fibrosis through modulation of the Wnt/β-catenin signaling pathway. *Ther Clin Risk Manag* **11**, 1371-1381.

Zhou, J., Ahmad, F., Parikh, S., Hoffman, N. E., Rajan, S., Verma, V. K., Song, J., Yuan, A., Shanmughapriya, S., Guo, Y., et al. (2016). Loss of Adult Cardiac Myocyte GSK-3 Leads to Mitotic Catastrophe Resulting in Fatal Dilated Cardiomyopathy. *Circulation Research* **118**, 1208-1222.

Zhu, W., Zhang, E., Zhao, M., Chong, Z., Fan, C., Tang, Y., Hunter, J. D., Borovjagin, A. V., Walcott, G. P., Chen, J. Y., et al. (2018). Regenerative Potential of Neonatal Porcine Hearts. *Circulation* **138**, 2809-2816.

Figures

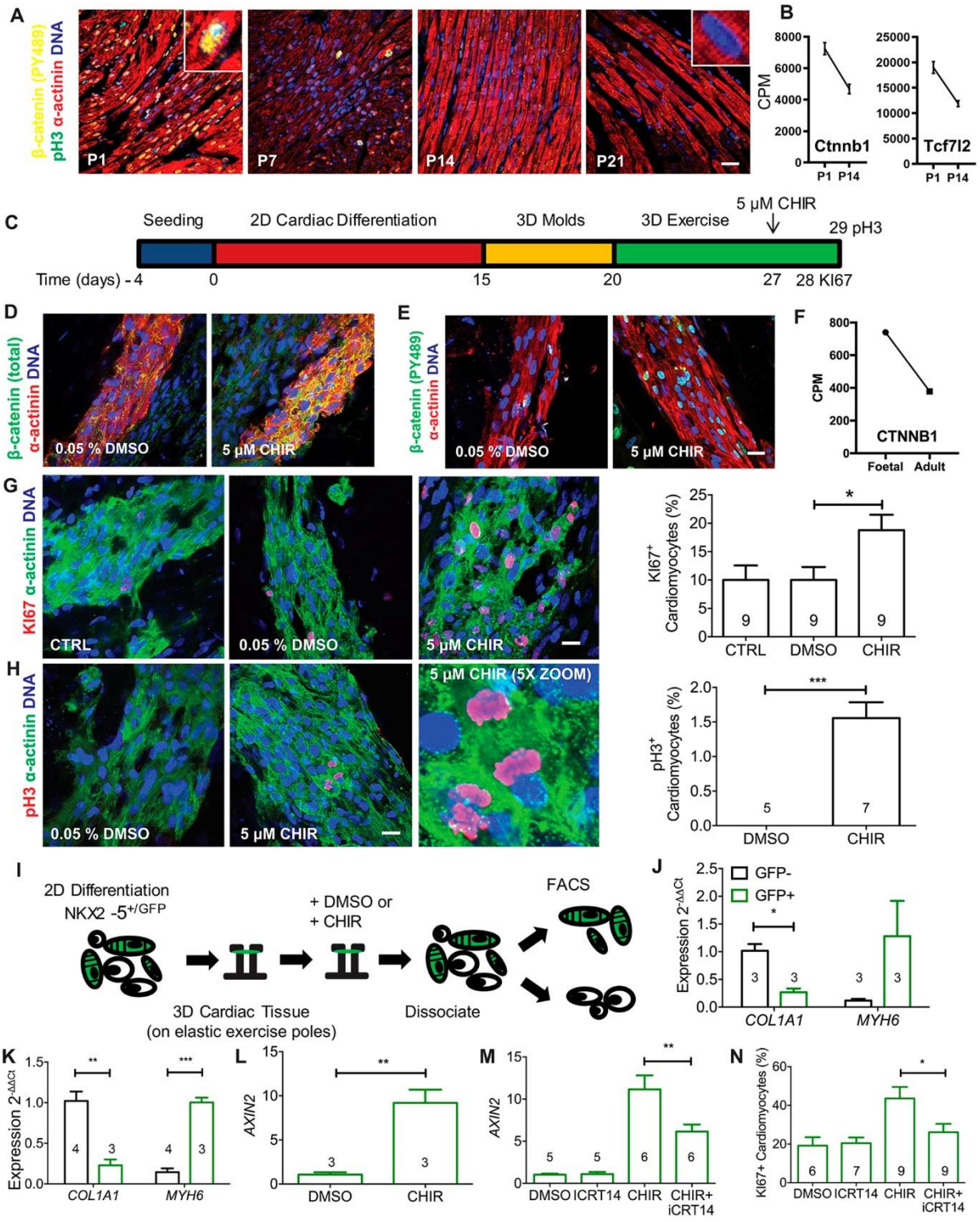

Figure 1. Wnt/β-catenin is developmentally shutdown in mouse heart and drives human ESC-derived cardiomyocyte proliferation.

(A) Nuclear expression of β-catenin is concomitantly downregulated with pH3 proliferating cardiomyocytes during postnatal cardiac maturation in mice. (B) Ctnnb1 and Tcf7l2 are downregulated in cardiomyocytes during postnatal development between P1 and P14. Data

obtained from cardiomyocyte nuclei RNA-seq from Quaife-Ryan et al., 2017 (GSE95764). n = 3 per group. Data represented as counts per million (CPM). (C) Activation of β-catenin in human hCOs results in activation of cardiomyocyte proliferation. The GSK3 inhibitor CHIR was used to activate β-catenin in these experiments and DMSO was used as a vehicle control. (D) Treatment of hCO with CHIR resulted in retention of inactive β-catenin at cell-cell junctions. (E) Treatment of hCO with CHIR resulted in active β-catenin in cardiomyocyte nuclei. (F) Human CTNNB1 is downregulated during cardiac maturation *in vivo*. RNA-seq samples available at GEO with accession GSE93841. (G) Treatment of hCO with CHIR resulted in induction of proliferation in cardiomyocytes after 24h using KI-67. Data pooled from 2 independent experiments. Statistical significance tested using ANOVA with Dunett's post-hoc test. 4784 cardiomyocytes were manually counted in these experiments. (H) Treatment of hCO with CHIR resulted in induction of proliferation of cardiomyocytes after 48h using pH3 as a marker of mitosis. Data pooled from 2 independent experiments. 2641 cardiomyocytes were manually counted in these experiments. (I) Schematic of strategy to purify cardiomyocytes from hCO generated using the NKX2-5GFP/+ human ESC line. (J) qPCR of target genes confirms separation of cell populations and purification of cardiomyocytes in the GFP+ fraction in both DMSO and (K) CHIR treated hCO at 24 h. qPCR data is normalized to GFP- cells for COL1A1 and GFP+ cells for αMHC. Data is 3-4 independent experiments. (L) qPCR of the β-catenin transcriptional target AXIN2 confirms transcriptional activation in cardiomyocytes (GFP+ fraction) in CHIR treated hCO at 24 h. Data is 3-4 independent experiments (M) Inhibition of β-catenin transcriptional activity using ICRT14 is confirmed via qPCR of AXIN2 in hCO after 24 h (N) ICRT14 inhibits CHIR induction of cardiomyocyte cell cycle in hCO after 24 h. The numbers in bar graphs represent the number of hCOs analysed in each group. Bars = 20 μm. P1 = 1 day old mice, P7 = 7 day old mice, P14 = 14 day old mice, P21 = 21 day old mice.

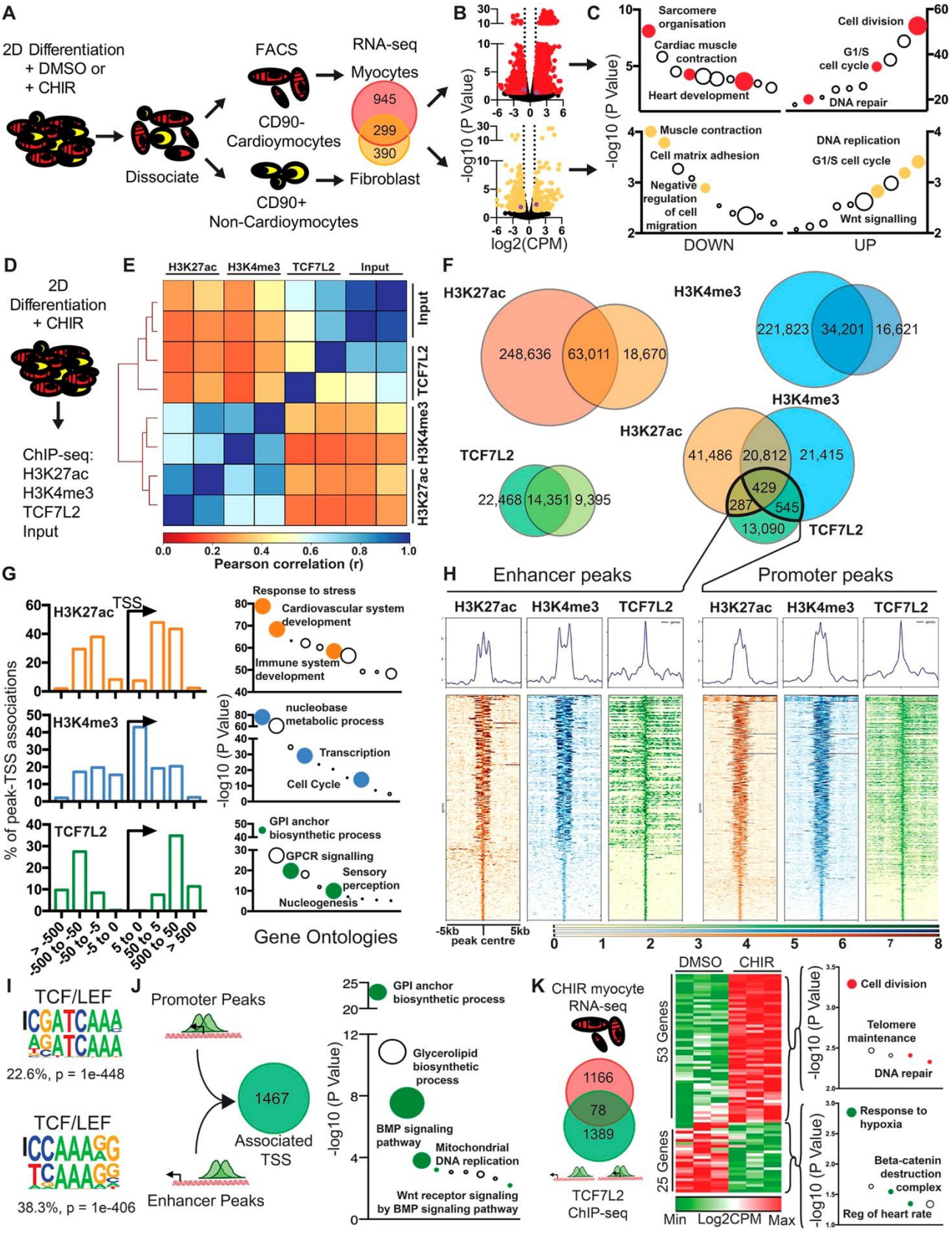

Figure 2. Defining the β-catenin signaling network in human ESC-derived cardiomyocytes.

(A) Schematic outline for isolating and performing RNA-seq on cardiomyocytes and CD90+ stromal cells from 2D differentiated human cells treated with CHIR or DMSO. This analysis identified a common network of 299 DEGs shared in cardiomyocytes and fibroblasts. N=3 experiments for all groups. (B) CHIR regulated 1244 cardiomyocyte genes (725 genes upregulated and 519 downregulated) and 689 fibroblast genes (298 upregulated and 391 downregulated). Significant genes are labelled in red or yellow for myocyte or stromal cells, respectively. 2 genes were differentially regulated in cardiomyocytes and stromal cells (highlighted in purple). (C) Treatment with CHIR stimulated cell-cycle gene ontologies in both myocytes and fibroblasts. Alternatively, gene ontologies involved in cell identity such as sarcomeric organisation and cell matrix adhesion where shut down in myocytes and stromal cells, respectively. (D) Schematic of ChIP-seq of H3K27ac, H3K4me3 and TCF7L2 in CHIR treated 2D cardiac cells. Promoter and enhancer loci were identified in 2D derived cardiomyocytes using H3K27ac and H3K4me3 ChIP-seq. n=2 experiments (E) Consistency between sample groups was assessed using Pearson correlation. (F) Venn diagrams of H3K27ac, K3K4me3 and TCF7L2 peaks. (G) The majority of TCF7L2 and H3K27ac peaks were situated distal to TSSs. H3K4me3 peaks were proximal to TSSs. GO of genes associated with H3K27ac, H3K4me3 and TCF7L2 peaks are displayed. (H) The distribution of H3K27ac, H3K4me3 and TCF7L2 peaks at TCF7L2 enhancers and promotors. (I) *De novo* motif analysis identified 2 TCF/LEF binding motifs in TCF7L2 enhancer and promoter peaks. The black bar highlights the *de novo* motifs and the associated known motif is beneath. The 2 motifs were found in 22.6% (top) and 38.3% (bottom) of peaks. (J) TCF7L2 enhancer and promoter peaks were associated with 1467 genes implicated in glycosylphosphatidylinositol synthesis, BMP signaling, mitochondrial DNA replication and Wnt/BMP signaling. (K) Of the 1244 CHIR DEGs, 78 were direct targets of TCF7L2. The 53 CHIR upregulated TCF target genes were associated with cell cycle gene ontologies and the 25 downregulated genes were associated with hypoxia and β-catenin destruction complex.

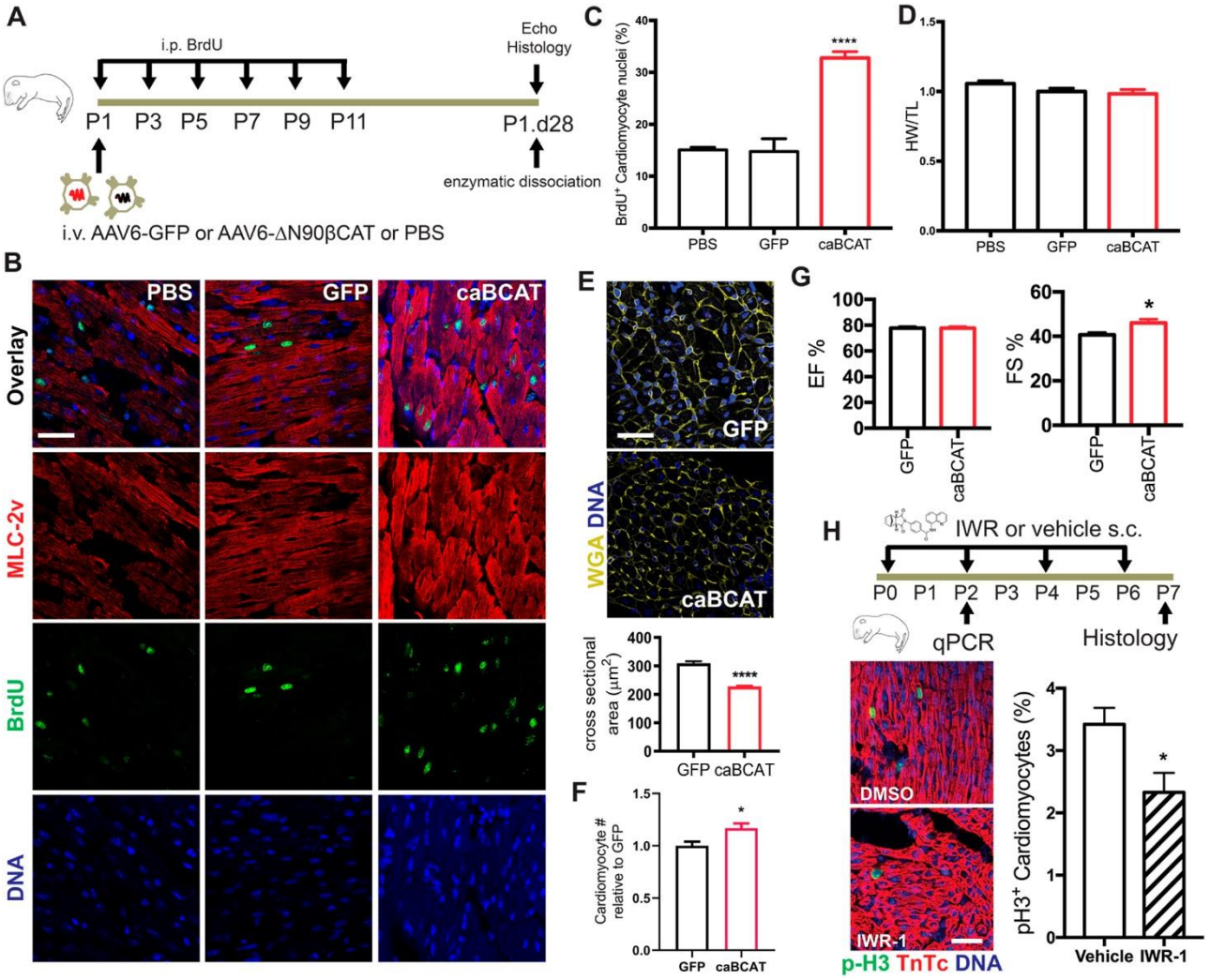

Figure 3. Wnt/β-catenin signaling drives neonatal cardiomyocyte proliferation *in vivo*.

(A) An experimental schematic for i.v. injection of PBS-only control, AAV6-GFP and AAV6-caBCAT in neonatal mice. Mice were pulsed with 100mg/kg 5-bromo-2'-deoxyuridine (BrdU) according to the schematic. (B) Representative images BrdU staining of PBS-only, GFP or caBCAT injected mice 28 days post injection (P1.d28). (C) caBCAT induces neonatal cardiomyocyte DNA synthesis in P1.d28 animals without a significant change in (D) heart weight:tibia length ratio. (E) caBCAT injected mice had reduced cardiomyocyte cell size. (F) Cardiomyocyte number was increased in caBCAT treated mice at day 28 following neonatal AAV injection compared to GFP controls. (G) Cardiac function (ejection fraction) was unaffected by caBCAT. (H) An experimental schematic of inhibition of β-catenin signaling with IWR-1 in neonatal mice (top panel). IWR-1 significantly reduced cardiomyocyte cell cycle (pH3+/TnTc+ cells) at P7. n = 6 for both groups for Panels B-E and G-H. n = 10 caBCAT and n = 11 GFP for Panel F. Bars = 40 μm.

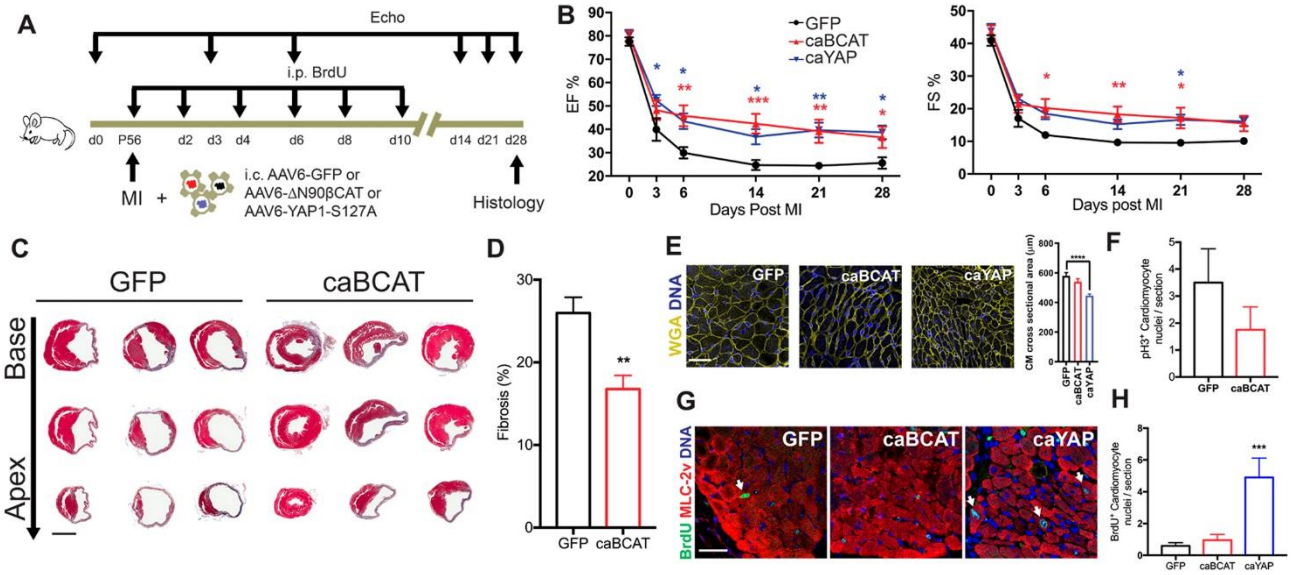

Figure 4. Constitutively active β-catenin exhibits cardioprotective rather than pro-proliferative effects in the infarcted adult myocardium.

(A) Schematic overview of AAV6-GFP, AAV6-caBCAT and AAV6-caYAP intramyocardial injection following MI of adult mice. Echocardiography was performed at d0, d3, d6, d14, d21 and day28 post MI. BrdU (100 mg/kg) was injected every second day for 6 days. All mice were sacrificed at MIP56.d28 for histology. (B) caBCAT and caYAP mitigated cardiac functional decline following MI as measured by ejection fraction and fractional shortening. At 4 weeks post infarction, ejection fractions of GFP, caBCAT and caYAP were: 26 ± 2%, 37 ± 5% and 39 ± 3%; and fractional shortening were: 10 ± 1%, 16 ± 2%, 16 ± 1%, respectively. (C) Masson's trichrome staining revealed infarct size reduction of caBCAT treated mice at 28 days post injection. Representative images of 3 hearts from each group are displayed from base to apex. Scale bar is 1 mm. (D) Quantification of fibrotic tissue showed a significant reduction of fibrotic tissue in caBCAT treated hearts. (E) Wheat germ agglutinin (WGA) staining and quantification of cardiomyocyte cross-sectional area in GFP, caBCAT and caYAP treated mice at 28 days post MI. The cross-sectional area for 6200 cardiomyocytes were individually counted for this analysis (200 cardiomyocytes per heart). Bar = 40 μm. (F) Mitotic cardiomyocytes (pH3+) were unaltered between GFP and caBCAT at MIP56.d3. (G) Representative images of BrdU+/MLC-2v+ cardiomyocytes in GFP, caBCAT and caYAP MIP56.d28 hearts. (H) Quantification of BrdU+/MLC-2v+ cardiomyocytes. caBCAT failed to increase the number of BrdU+ cardiomyocytes. Bar = 40 μm. For panels B-E and G-H, n = 10 AAV6-GFP, n = 11 AAV6-caBCAT, n = 10 AAV6-caYAP. For panel F, n = 4 for both groups

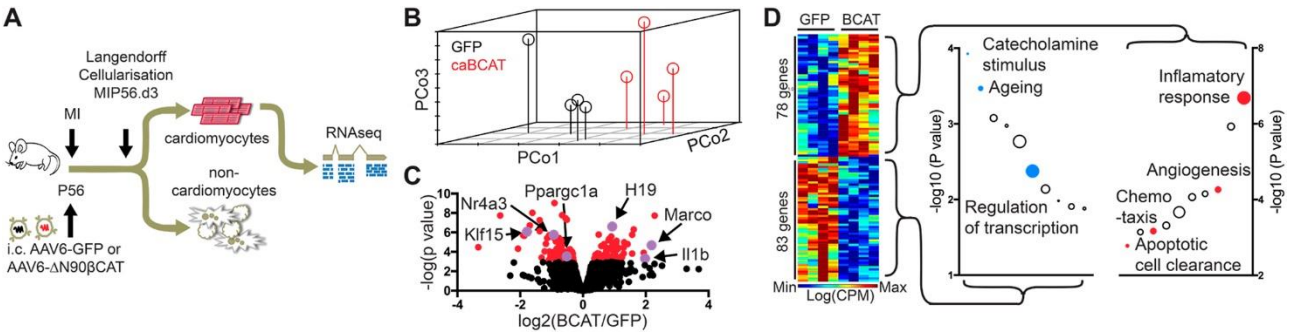

Figure 5. The β-catenin cardioprotective gene program in adult cardiomyocytes.

(A) A schematic detailing the isolation and RNA-seq of caBCAT treated cardiomyocytes from MI mouse hearts. Mice were intramyocardially injected with either AAV6-GFP or AAV6-caBCAT at the time of MI surgery. After 3 days, cardiomyocytes were isolated and RNA-seq performed. (B) 3D Principal coordinate analysis of caBCAT and GFP cardiomyocytes. Black = GFP treated cardiomyocytes, red = caBCAT treated cardiomyocytes. (C) caBCAT differentially regulated 161 genes. The volcano plot depicts differentially regulated genes between caBCAT and GFP treated cardiomyocytes. Significantly regulated genes are displayed in red and genes of interest are highlighted in purple. (D) caBCAT upregulated 76 and downregulated 83 cardiomyocyte genes. Downregulated genes were associated with metabolic processes and transcription. Inflammatory and angiogenic genes were upregulated. n = 4 for both groups.

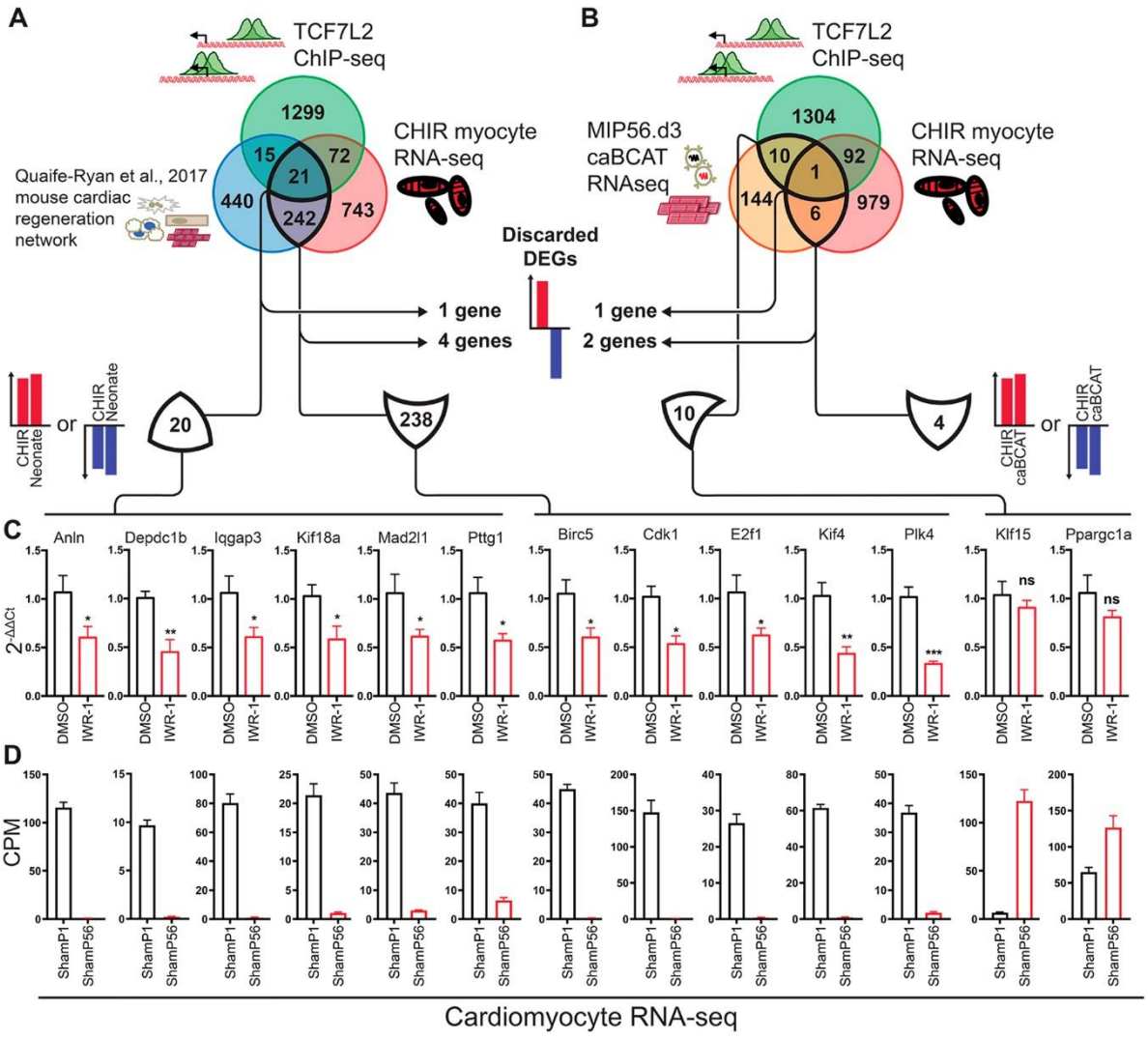

Figure 6. β-catenin drives distinct transcriptional programs in regenerative and non-regenerative cardiomyocytes.

(A) Direct targets of TCF7L2 in multiple datasets human cardiomyocytes, CHIR-regulated genes and genes from the cardio-regenerative gene program described in Quaife-Ryan et al., (2017) were compared. 263 genes were common to CHIR and regeneration networks and 21 were direct targets of TCF7L2. 5 genes were not regulated in the same direction (e.g. upregulated in the regeneration network but downregulated in CHIR) were discarded. (B) 1 gene was a direct target of TCF7L2 and coregulated in both the CHIR and caBCAT-treated adult cardiomyocyte networks. Genes that were not regulated in the same direction in caBCAT-treated myocytes and CHIR were discarded. (C) Several regeneration network, CHIR regulated genes and TCF7L2 direct targets were validated by qPCR in IWR-1 treated neonatal hearts, including several that were direct targets of TCF7L2. qPCR data represented as $2^{-\Delta\Delta Ct}$, n = 5 for DMSO and n = 6 for IWR-1 (D) Many CHIR-responsive genes were downregulated during postnatal cardiomyocyte development. None of the adult

caBCAT regulated genes were downregulated in IWR-1 treated neonatal hearts, potentially because of low level expression in neonatal cardiomyocytes. Data obtained from RNA-seq of isolated neonatal (ShamP1) and adult (ShamP56) cardiomyocytes and represented as CPM (GSE95755)(Quaife-Ryan et al., 2017). n = 4 for both groups.

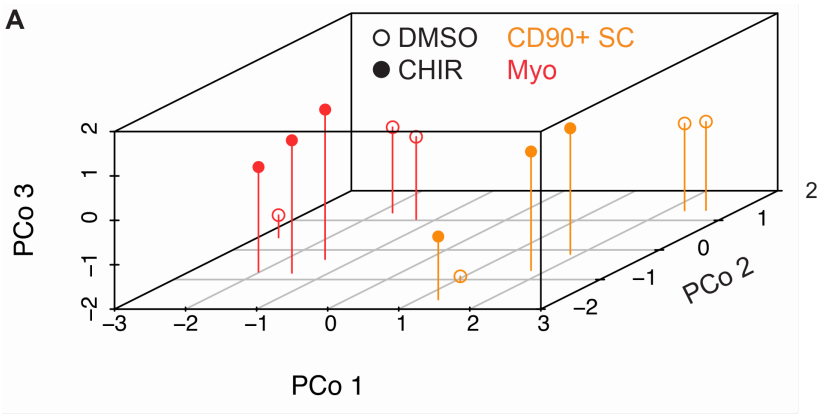

Figure S1. Cardiomyocytes and CD90+ stromal cells remain transcriptionally distinct following CHIR treatment.

3D PCoA analysis of CHIR or DMSO treated 2D derived cardiomyocytes and CD90+ stromal cells. n = 3 for all groups. Red = cardiomyocytes, Orange = CD90+ stromal cells

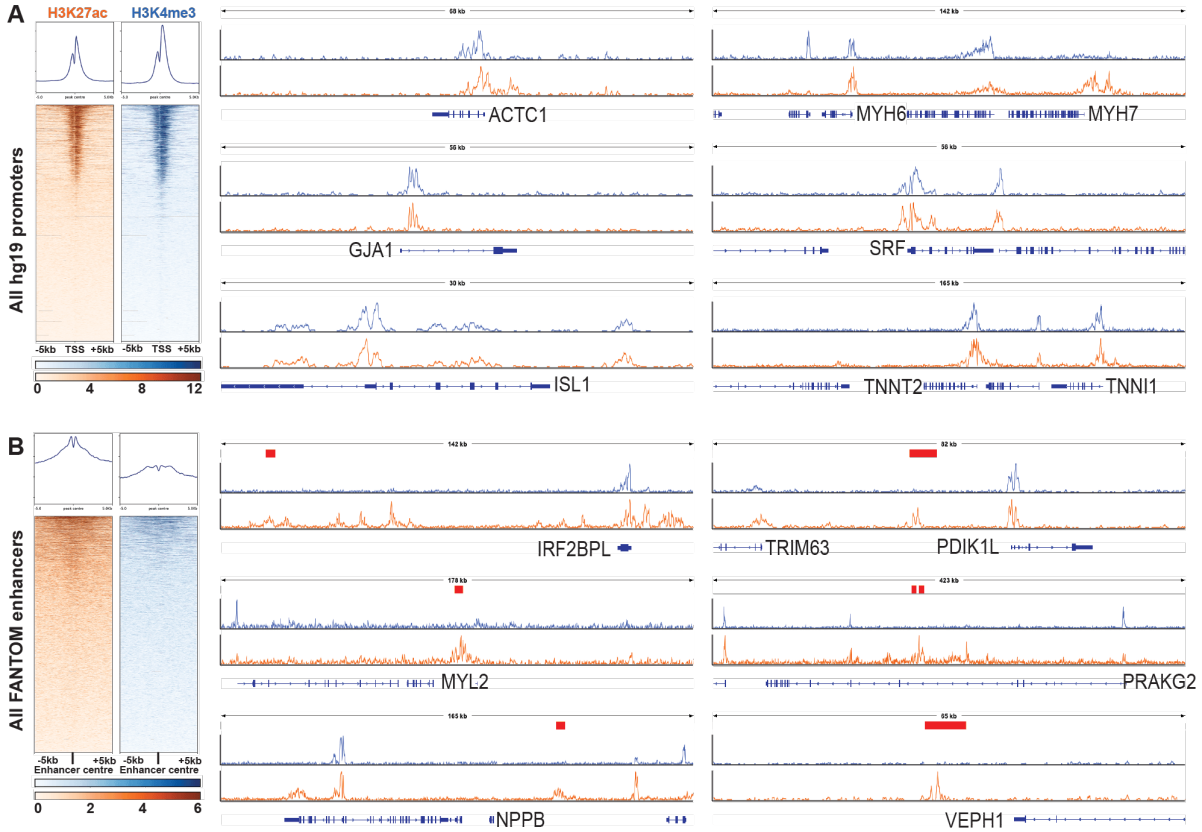

Figure S2. H3K4me3 and H3K27ac peaks at well-characterised cardiomyocyte-specific promoters and enhancers

(A) Left panel displays a heatmap of ChIP-seq H3K4me3 and H3K27ac peaks ±5 kb from all promoters annotated in the hg19 genome assembly. H3K4me3 and H3K27ac peaks surrounding cardiomyocyte-related genes. (B) Left panel is a heatmap of H3K4me3 and H3K27ac heatmaps at all enhancers identified by the FANTOM consortium (Arner et al., 2015). Right panel displays genome tracks surrounding known cardiomyocyte genes. Red bars indicate validated human cardiac enhancer sites (Spurrell et al., 2019; Visel et al., 2009). Blue = H3K4me3, Orange = H3K27ac

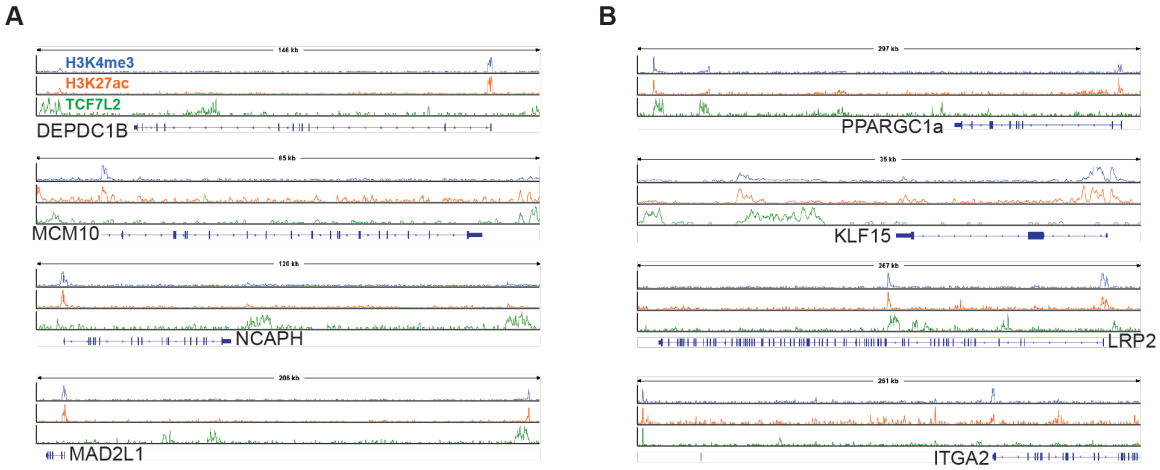

Figure S3. Proximal and distal localisation of TCF7L2 to CHIR-regulated genes

Genome tracks surrounding CHIR-regulated direct targets of TCF7L2 in 2D derived human cardiomyocytes. H3K4me3, H3K27ac, and TCF7L2 ChIP-seq peaks are displayed in blue, orange and green, respectively.

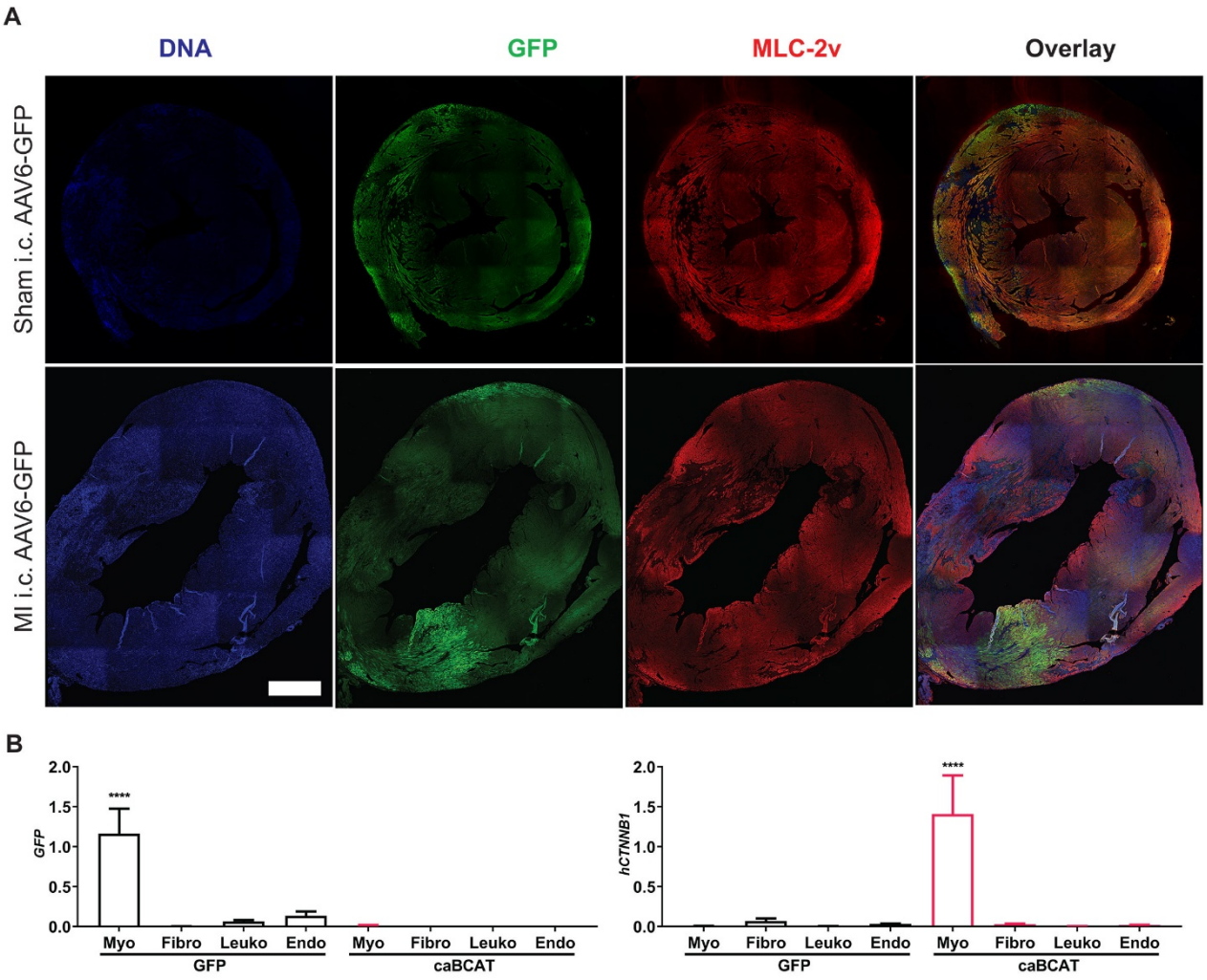

Figure S4. AAV6 delivered constructs are specifically expressed in border zone cardiomyocytes following intracardiac injection in mice.

(A) Confocal tile scan images of AAV6-GFP injected hearts following Sham or MI surgery. Each heart was injected with 1 x 10^{11} viral particles at 4 sites surrounding the infarct. Representative images shown. Images taken 3 days post-surgery and intracardiac injections. Scale bar = 1 mm. (B) qPCR for human *CTNNB1* and GFP in cardiomyocytes, fibroblasts, leukocytes and endothelial cells isolated 3 days post AAV6-GFP and AAV6-caBCAT injection. n = 4.

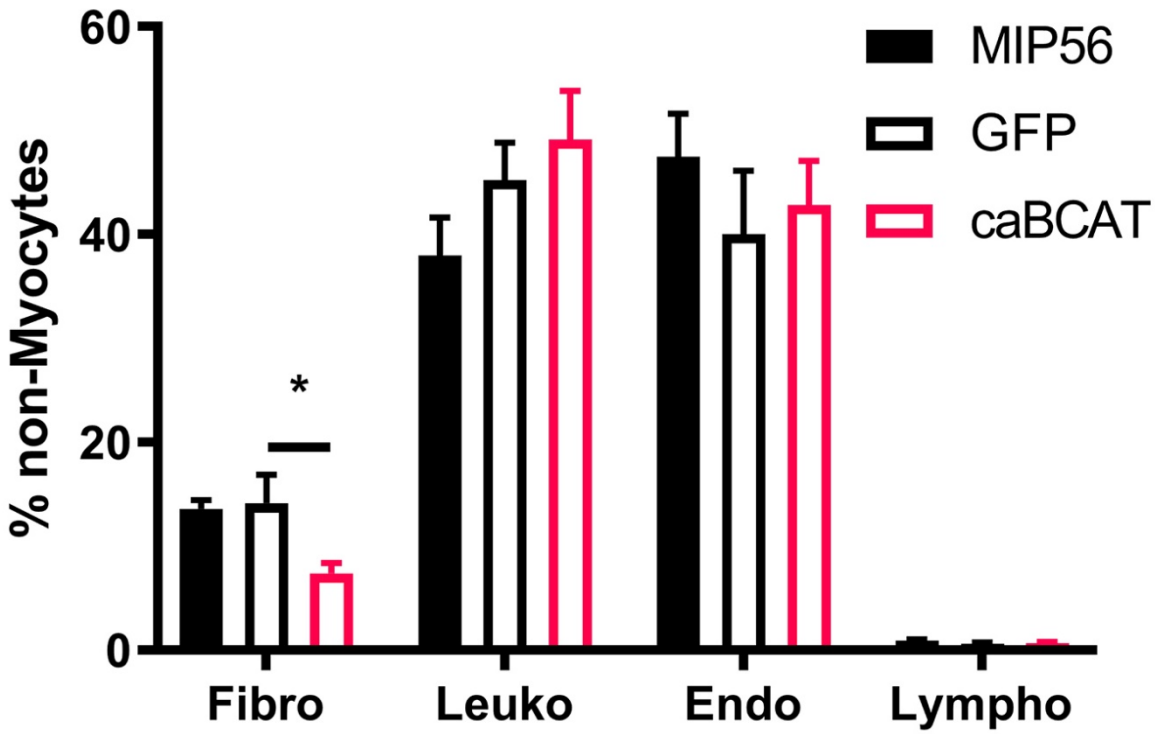

Figure S5. Fibroblast number is reduced in caBCAT treated hearts at day 3 post MI.

Fibroblasts, leukocytes endothelial cells and lymphatic endothelial cells well isolated from MIP56 (no i.c. injection), AAV6-GFP and AAV-caBCAT injected hearts at day 3 post MI. The fibroblast population was diminished in caBCAT treated hearts. n = 4.

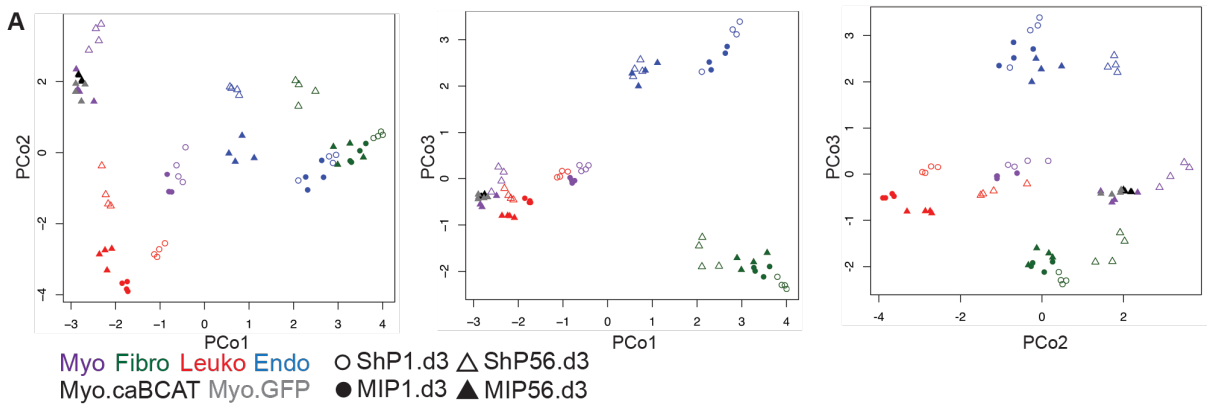

Figure S6. The transcriptional identity of adult cardiomyocytes is unaltered by caBCAT

3D principal coordinate analysis (PCoA) comparing MIP56.d3 caBCAT or GFP treated cardiomyocytes and the entire multicellular RNA-seq dataset (Quaife-Ryan et al., 2017). n = 4 for all groups. Purple = MIP56.d3 cardiomyocytes, green = MIP56.d3 fibroblasts, red = MIP56.d3 leukocytes, blue = MIP56.d3 endothelial cells, black = MIP56.d3 caBCAT cardiomyocytes and gray = MIP56.d3 GFP cardiomyocytes. Open circles = ShP1.d3, closed circules = MIP1.d3, open triangles = ShP56.d3, closed triangles = MIP56.d3.

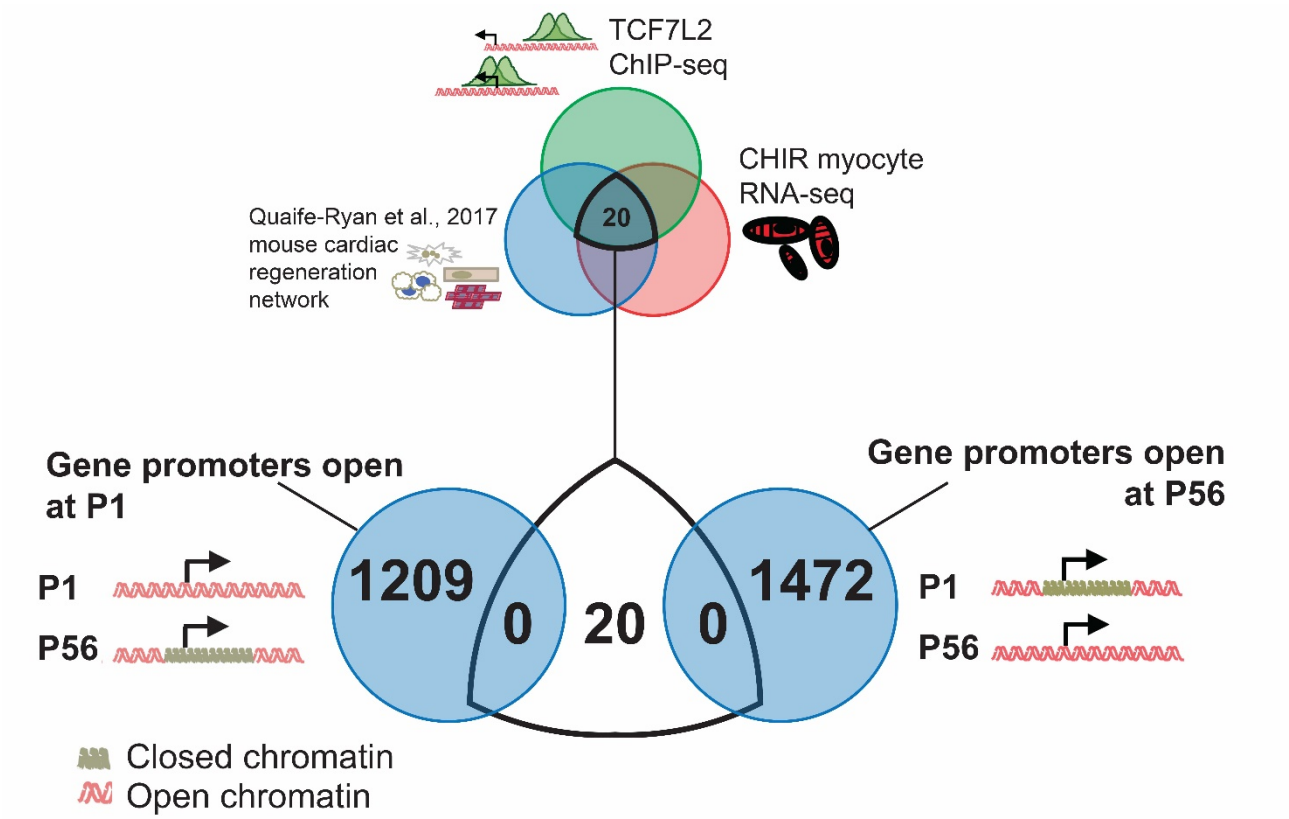

Figure S7. β-catenin target gene promoters are not epigenetically repressed during postnatal cardiomyocyte maturation

The 20 β-catenin immature myocyte target genes identified in Fig. 6 were intersected with P1 and P56 ATAC-seq cardiomyocyte datasets. Chromatin accessibility was unaltered around these target gene promoters during cardiomyocyte development. ATAC-seq datasets obtained from (Quaife-Ryan et al., 2017) (GSE95764). For each ATAC-seq, n = 3.

Table S1. Antibodies used in this study

Antibody	Species	Samples	Company	Cat No	Dilution
Alexa Fluor 488 goat anti-chicken IgG (H+L)	Goat IgG	Secondary antibody	Life Technologies	A-11039	1:33
Alexa Fluor 488 goat anti-mouse IgG (H+L)	Goat IgG	Secondary antibody	Life Technologies	A-11029	1:10
Alexa Fluor 488 goat anti-mouse IgM (μ chain)	Goat IgG	Secondary antibody	Life Technologies	A-21042	1:33
Alexa Fluor 488 goat anti-rabbit IgG (H+L)	Goat IgG	Secondary antibody	Life Technologies	A-11034	1:67
Alexa Fluor 555 goat anti-mouse IgG (H+L)	Goat IgG	Secondary antibody	Life Technologies	A-21422	1:100
Alexa Fluor 555 goat anti-rabbit IgG (H+L)	Goat IgG	Secondary antibody	Life Technologies	A-21428	1:100
Alexa Fluor 633 goat anti-rabbit IgG (H+L)	Goat IgG	Secondary antibody	Life Technologies	A-21070	1:100
anti-BrdU	IgG1, kappa light chain	IF imaging	DSHB	G3G4 (anti-BrdU)	1:100
Anti-MLC-2v	Rabbit IgG	IF imaging	Proteintech	10906-1-AP	1:1000
Anti-phospho-Histone H3 (Ser10)	Rabbit polyclonal	IF imaging	Millipore	06-570	1:100
Anti-TnTc	Mouse IgG1	IF imaging	Thermo Scientific	MS-295-P0	1:100
anti-β-catenin (PY489)	Mouse IgM	IF imaging	DSHB	PY489-B-catenin	1:400
CD31-BV421	Rat IgG2a	Mouse FACS	BioLegend	102423	1:100
CD45-FITC	Rat IgG2b	Mouse FACS	Miltenyi Biotec	130-102-778	1:200
CD90	Mouse IgG2A	hPSC FACS	RnD Systems	MAB2067	1:400
CD90-APC	Rat IgG2c	Mouse FACS	ThermoFisher	A14727	1:400
GFP	Chicken polyclonal	IF imaging	Abcam	ab13970	1:400
Ki-67 (D3B5)	Rabbit IgG	IF imaging	Cell Signalling Technology	9129	1:400
Podoplanin-PE/Cy7	Syrian Hamster IgG	Mouse FACS	BioLegend	127411	1:400
Wheat germ agglutinin, Alexa Fluor 488	NA	IF imaging	ThermoFisher Scientific	W11261	1:400
α-Actinin (clone EA-53)	Mouse IgG1	IF imaging	ThermoFisher	A-21070	1:400

Table S2 Primers for quantitative PCR

Gene	Accession	Forward	Reverse	Size (bp)
Human qPCR primers				
18s	18s repeat sequence	TCGAGGCCCTGTAATTGGAA	CCCTCCAATGGATCCTCGTT	61
COL1a1	ENSG00000108821	GTGCTAAAGGTGCCAATGGT	ACCAGGTTCACCGCTGTTAC	128
HPRT1	ENSG00000165704	AACCTCTCGGCTTTCCCG	TCACTAATCACGACGCCAGG	150
MYH6	ENSG00000197616	CTCCTCCTACGCAACTGC	ACACCGTCTGGAAGGATGA	83
CTNNB1	ENSG00000168036	CTTACACCCACCATCCCACT	TGATGTGCACGAACAAGCAA	144
Mouse qPCR primers				
18s	18s repeat sequence	TCGAGGCCCTGTAATTGGAA	CCCTCCAATGGATCCTCGTT	61
Anln	ENSMUSG00000036777	ATGTTAGTGGCTTTGGTGCC	TGGGATTCTTTCGCCTCTCA	102
Birc5	ENSMUSG00000017716	AACCCGATGACAACCCGAT	TGGTCTCCTTTGCAATTTTGTTC	150
Cdk1	ENSMUSG00000019942	ACACACACGAGGTAGTGACG	AACCGGAGTGGAGTAACGAG	80
Depdc1b	ENSMUSG00000021697	TTGTGATTCAAACTGCGGCG	TCCACTGTTTCATTCCACAGC	143
E2f1	ENSMUSG00000027490	ACCCAGGGAAAGGTGTGAAA	CAAGAAGCGTTTGGTGGTCA	80
Hprt	ENSMUSG00000025630	AGGCCAGACTTTGTTGGATTTGAA	CAACTTGCGCTCATCTTAGGCTTT	150
Iqgap3	ENSMUSG00000028068	GAGCTCGGACAGCCTATGAGC	AGCCGGCAGAGGTACTGATA	88
Kif18a	ENSMUSG00000027115	GTGGATTTGCCAAACGCATTC	TTTATAGCCCACTTTCAGTCTGT	80
Kif4	ENSMUSG00000034311	CCAGCAAACAGAAACCCCAT	AAGGTTTGGGCTTAGGTGGA	87
Klf15	ENSMUSG00000030087	GGAGAGCGGGGAGAGC	TGTGGTGACTGGACTCCG	148
Mad2l1	ENSMUSG00000029910	GAAGAATCGGGACCGCAA	CAGACCAAACGAACCGTCTC	138
Plk4	ENSMUSG00000025758	CGTAGAGAAGGCGTCCTGAT	TAAAGTCCTCGATCCTCTCCC	143
Ppargc1a	ENSMUSG00000029167	CTCTCAGTAAGGGGCTGGTT	CAGCACACTCTATGTCACTCC	150
Pttg1	ENSMUSG00000020415	TGGCGCAGTCTTCGAGTAAT	ATCCTTAGATGCCAAACGGC	91
Miscellaneous qPCR Primers				
GFP	-	AAGGGCATCGACTTCAAGG	TGCTTGTCGGCCATGATATAG	95

Table S3 Summary of RNA-seq mapping efficiencies of MIP56 caBCAT experiment

Sample	number of reads	%uniquely mapped reads	%multi-mapped reads	%unmapped
Myo_GFP_1	65812645	71.21%	25.52%	3.27%
Myo_GFP_2	58613420	69.79%	26.80%	3.41%
Myo_GFP_3	67027367	71.61%	24.98%	3.41%
Myo_GFP_4	65004587	71.52%	24.60%	3.88%
Myo_BCAT_1	71693147	71.26%	25.37%	3.37%
Myo_BCAT_2	74057324	73.35%	23.83%	2.82%
Myo_BCAT_3	67597492	70.32%	26.50%	3.18%
Myo_BCAT_4	65687633	69.98%	26.81%	3.21%

Table S4 Summary of mapping efficiencies for ChIP-seq

Sample	number of reads	%uniquely mapped reads	%multi-mapped reads	%unmapped
H3K27ac_1	40192146	69.93%	28.52%	1.55%
H3K27ac_2	73153197	76.80%	22.26%	0.94%
H3K4me3_1	42817370	67.22%	31.03%	1.74%
H3K4me3_2	71856079	75.62%	22.83%	1.54%
Input_1	82802143	71.20%	27.28%	1.53%
Input_2	85319259	73.57%	24.84%	1.59%
TCF7l2_1	66744568	68.12%	29.74%	2.09%
TCF7l2_2	77627877	68.35%	28.43%	3.22%

Table S5. Bioinformatic programs used in this study

Software	Reference	RRID
NCBI Primer-BLAST	(Ye et al., 2012)	RRID:SCR_003095
Trimmomatic	(Bolger et al., 2014)	RRID:SCR_011848
STAR	(Dobin et al., 2013)	RRID:SCR_015899
HTSeq-count	(Anders et al., 2015)	RRID:SCR_011867
EdgeR	(Robinson et al., 2010)	RRID:SCR_012802
DAVID	(Huang et al., 2007)	RRID:SCR_001881
GENE-E	Broad Institute	N/A
Bowtie2	(Langmead and Salzberg, 2012)	RRID:SCR_005476
MACS2	(Zhang et al., 2008)	RRID:SCR_013291
GenomicRanges	(Lawrence et al., 2013)	RRID:SCR_000025
deepTools2	(Ramírez et al., 2016)	RRID:SCR_016366
GREAT	(McLean et al., 2010)	RRID:SCR_005807
HOMER	(Heinz et al., 2010)	RRID:SCR_010881

References:

Anders, S., Pyl, P. T. and Huber, W. (2015). HTSeq--a Python framework to work with high-throughput sequencing data. *Bioinformatics* **31**, 166-169.

Arner, E., Daub, C. O., Vitting-Seerup, K., Andersson, R., Lilje, B., Drabløs, F., Lennartsson, A., Rönnerblad, M., Hrydziuszko, O., Vitezic, M., et al. (2015). Gene regulation. Transcribed enhancers lead waves of coordinated transcription in transitioning mammalian cells. *Science (New York, N.Y.)* **347**, 1010-1014.

Bolger, A. M., Lohse, M. and Usadel, B. (2014). Trimmomatic: a flexible trimmer for Illumina sequence data. *Bioinformatics* **30**, 2114-2120.

Dobin, A., Davis, C. A., Schlesinger, F., Drenkow, J., Zaleski, C., Jha, S., Batut, P., Chaisson, M. and Gingeras, T. R. (2013). STAR: ultrafast universal RNA-seq aligner. *Bioinformatics* **29**, 15-21.

Heinz, S., Benner, C., Spann, N., Bertolino, E., Lin, Y. C., Laslo, P., Cheng, J. X., Murre, C., Singh, H. and Glass, C. K. (2010). Simple combinations of lineage-determining transcription factors prime cis-regulatory elements required for macrophage and B cell identities. *Molecular Cell* **38**, 576-589.

Huang, D. W., Sherman, B. T., Tan, Q., Collins, J. R., Alvord, W. G., Roayaei, J., Stephens, R., Baseler, M. W., Lane, H. C. and Lempicki, R. A. (2007). The DAVID Gene Functional Classification Tool: a novel biological module-centric algorithm to functionally analyze large gene lists. *Genome biology* **8**, R183-116.

Langmead, B. and Salzberg, S. L. (2012). Fast gapped-read alignment with Bowtie 2. *Nature Methods* **9**, 357-359.

Lawrence, M., Huber, W., Pagès, H., Aboyoun, P., Carlson, M., Gentleman, R., Morgan, M. T. and Carey, V. J. (2013). Software for computing and annotating genomic ranges. *PLoS computational biology* **9**, e1003118.

McLean, C. Y., Bristor, D., Hiller, M., Clarke, S. L., Schaar, B. T., Lowe, C. B., Wenger, A. M. and Bejerano, G. (2010). GREAT improves functional interpretation of cis-regulatory regions. *Nature Biotechnology* **28**, 495-501.

Quaife-Ryan, G. A., Sim, C. B., Ziemann, M., Kaspi, A., Rafehi, H., Ramialison, M., El-Osta, A., Hudson, J. E. and Porrello, E. R. (2017). Multicellular Transcriptional Analysis of Mammalian Heart Regeneration. *Circulation* **136**, 1123-1139.

Ramírez, F., Ryan, D. P., Grüning, B., Bhardwaj, V., Kilpert, F., Richter, A. S., Heyne, S., Dündar, F. and Manke, T. (2016). deepTools2: a next generation web server for deep-sequencing data analysis. *Nucleic acids research* **44**, W160-165.

Robinson, M. D., McCarthy, D. J. and Smyth, G. K. (2010). edgeR: a Bioconductor package for differential expression analysis of digital gene expression data. *Bioinformatics* **26**, 139-140.

Spurrell, C. H., Barozzi, I., Mannion, B. J., Blow, M. J., Fukuda-Yuzawa, Y., Afzal, S. Y., Akiyama, J. A., Afzal, V., Tran, S., Plajzer-Frick, I., et al. (2019). Genome-Wide Fetalization of Enhancer Architecture in Heart Disease. *bioRxiv*, 591362.

Visel, A., Blow, M. J., Li, Z., Zhang, T., Akiyama, J. A., Holt, A., Plajzer-Frick, I., Shoukry, M., Wright, C., Chen, F., et al. (2009). ChIP-seq accurately predicts tissue-specific activity of enhancers. *Nature* **457**, 854-858.

Ye, J., Coulouris, G., Zaretskaya, I., Cutcutache, I., Rozen, S. and Madden, T. L. (2012). Primer-BLAST: A tool to design target-specific primers for polymerase chain reaction. *BMC Bioinformatics* **13**, 134.

Zhang, Y., Liu, T., Meyer, C. A., Eeckhoute, J., Johnson, D. S., Bernstein, B. E., Nusbaum, C., Myers, R. M., Brown, M., Li, W., et al. (2008). Model-based analysis of ChIP-Seq (MACS). *Genome biology* **9**, R137.

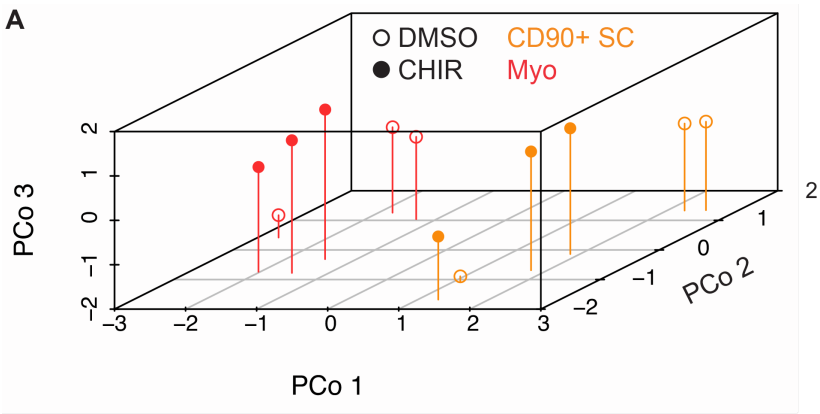

Figure S1. Cardiomyocytes and CD90+ stromal cells remain transcriptionally distinct following CHIR treatment.

3D PCoA analysis of CHIR or DMSO treated 2D derived cardiomyocytes and CD90+ stromal cells. n = 3 for all groups. Red = cardiomyocytes, Orange = CD90+ stromal cells

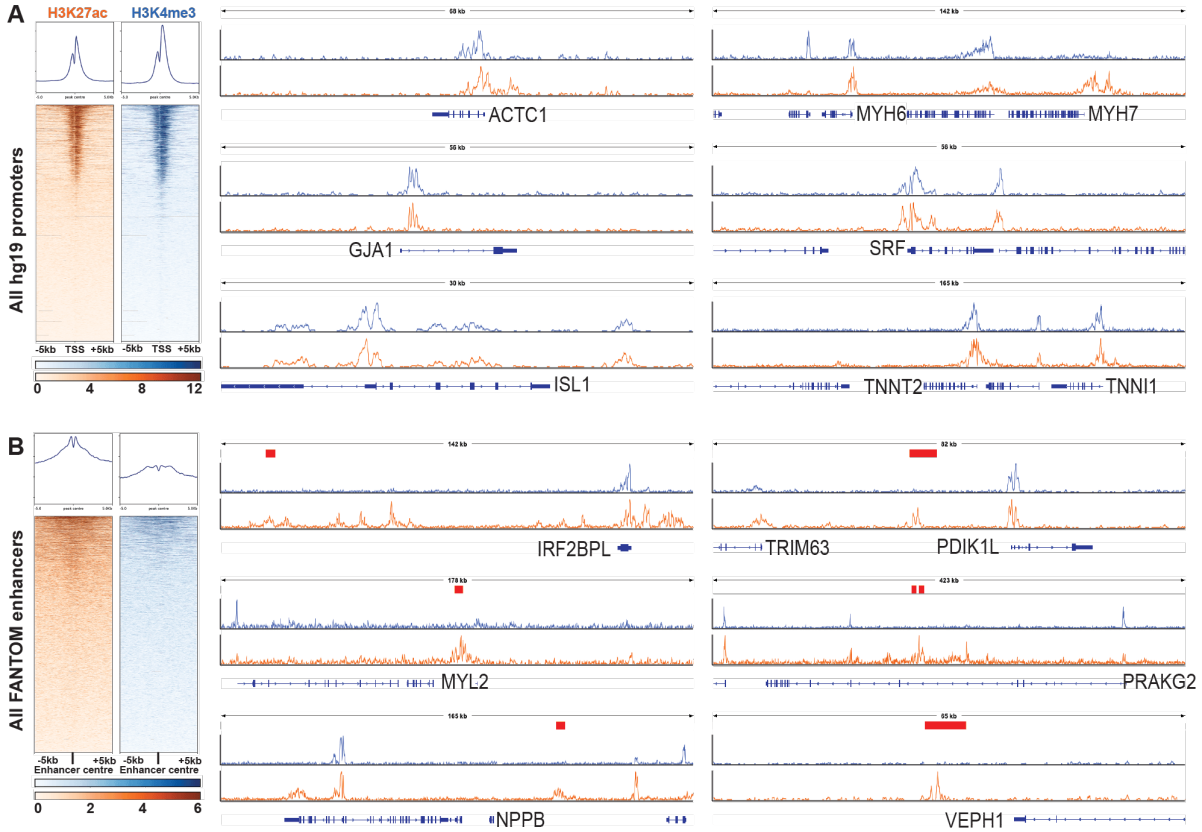

Figure S2. H3K4me3 and H3K27ac peaks at well-characterised cardiomyocyte-specific promoters and enhancers

(A) Left panel displays a heatmap of ChIP-seq H3K4me3 and H3K27ac peaks ±5 kb from all promoters annotated in the hg19 genome assembly. H3K4me3 and H3K27ac peaks surrounding cardiomyocyte-related genes. (B) Left panel is a heatmap of H3K4me3 and H3K27ac heatmaps at all enhancers identified by the FANTOM consortium (Arner et al., 2015). Right panel displays genome tracks surrounding known cardiomyocyte genes. Red bars indicate validated human cardiac enhancer sites (Spurrell et al., 2019; Visel et al., 2009). Blue = H3K4me3, Orange = H3K27ac

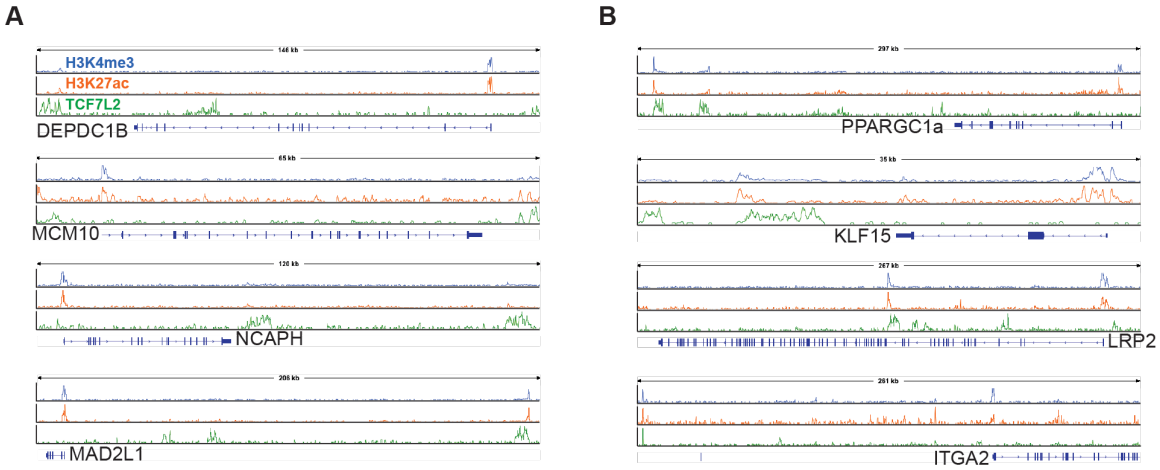

Figure S3. Proximal and distal localisation of TCF7L2 to CHIR-regulated genes

Genome tracks surrounding CHIR-regulated direct targets of TCF7L2 in 2D derived human cardiomyocytes. H3K4me3, H3K27ac, and TCF7L2 ChIP-seq peaks are displayed in blue, orange and green, respectively.

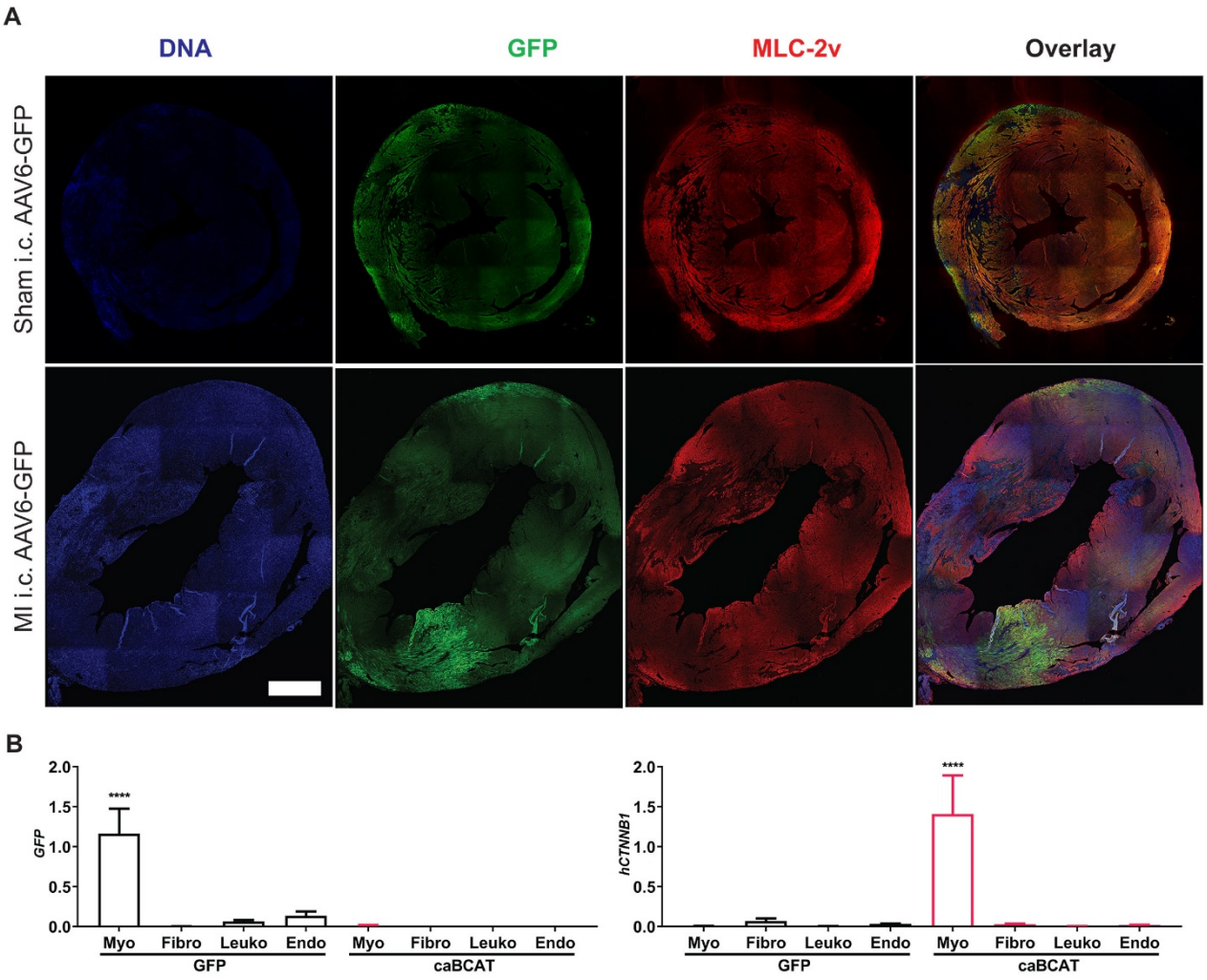

Figure S4. AAV6 delivered constructs are specifically expressed in border zone cardiomyocytes following intracardiac injection in mice.

(A) Confocal tile scan images of AAV6-GFP injected hearts following Sham or MI surgery. Each heart was injected with 1 x 10^{11} viral particles at 4 sites surrounding the infarct. Representative images shown. Images taken 3 days post-surgery and intracardiac injections. Scale bar = 1 mm. (B) qPCR for human *CTNNB1* and GFP in cardiomyocytes, fibroblasts, leukocytes and endothelial cells isolated 3 days post AAV6-GFP and AAV6-caBCAT injection. n = 4.

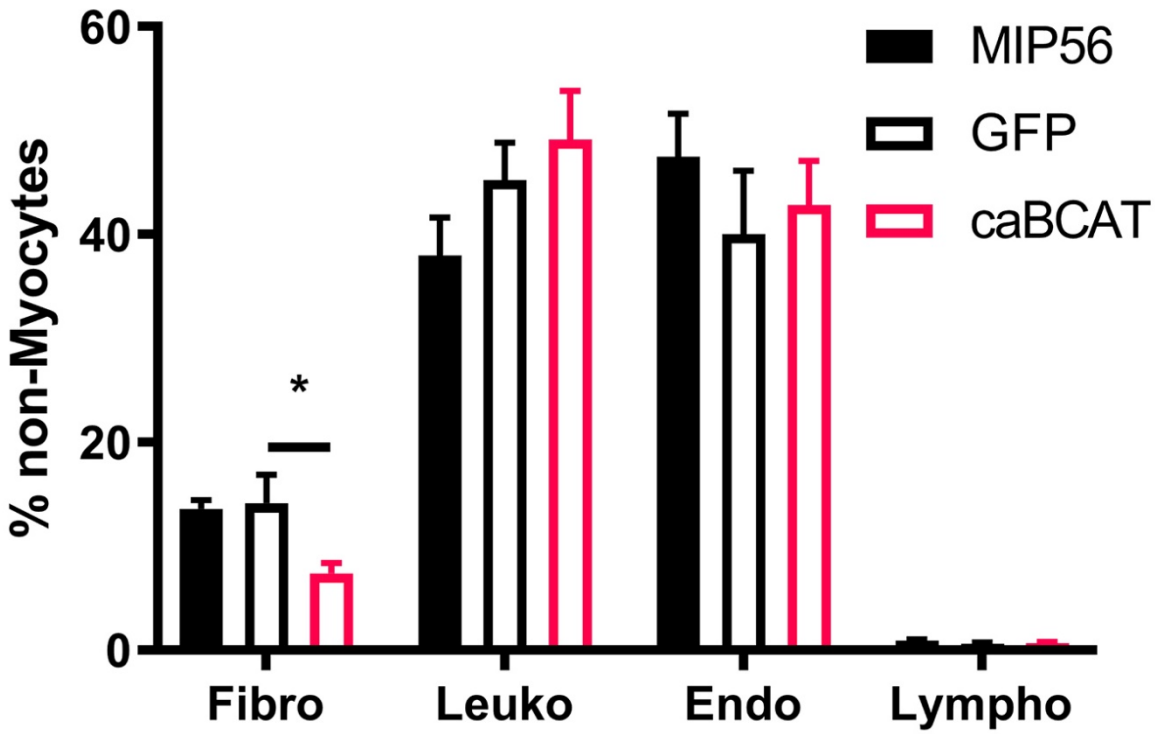

Figure S5. Fibroblast number is reduced in caBCAT treated hearts at day 3 post MI.

Fibroblasts, leukocytes endothelial cells and lymphatic endothelial cells well isolated from MIP56 (no i.c. injection), AAV6-GFP and AAV-caBCAT injected hearts at day 3 post MI. The fibroblast population was diminished in caBCAT treated hearts. n = 4.

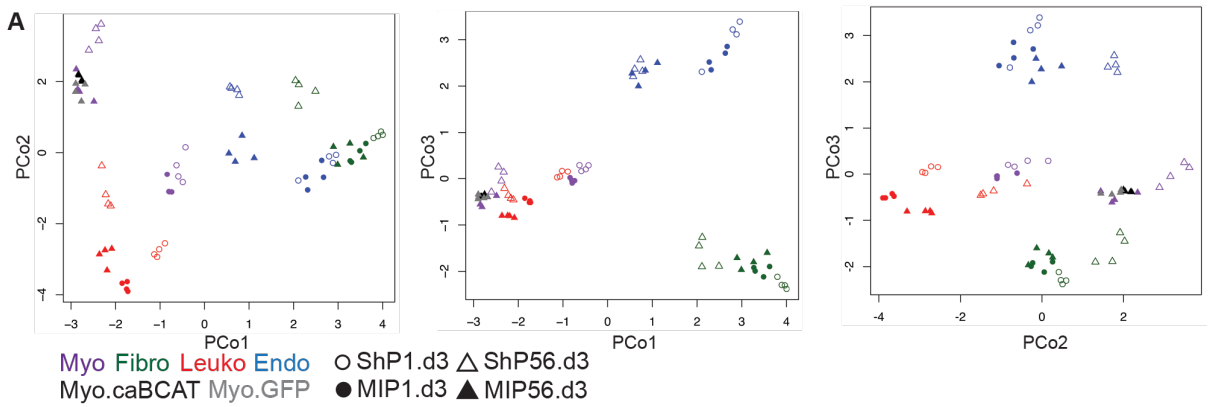

Figure S6. The transcriptional identity of adult cardiomyocytes is unaltered by caBCAT

3D principal coordinate analysis (PCoA) comparing MIP56.d3 caBCAT or GFP treated cardiomyocytes and the entire multicellular RNA-seq dataset (Quaife-Ryan et al., 2017). n = 4 for all groups. Purple = MIP56.d3 cardiomyocytes, green = MIP56.d3 fibroblasts, red = MIP56.d3 leukocytes, blue = MIP56.d3 endothelial cells, black = MIP56.d3 caBCAT cardiomyocytes and gray = MIP56.d3 GFP cardiomyocytes. Open circles = ShP1.d3, closed circules = MIP1.d3, open triangles = ShP56.d3, closed triangles = MIP56.d3.

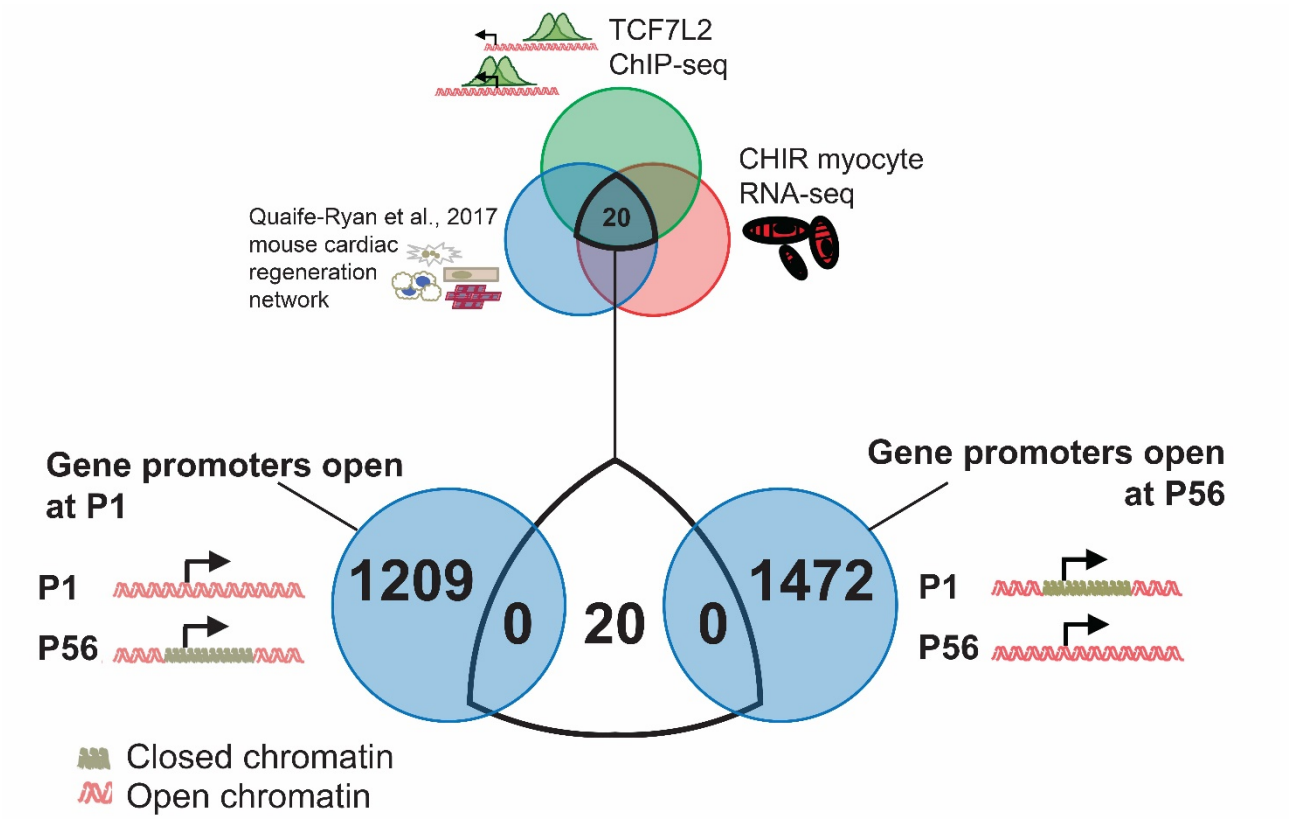

Figure S7. β-catenin target gene promoters are not epigenetically repressed during postnatal cardiomyocyte maturation

The 20 β-catenin immature myocyte target genes identified in Fig. 6 were intersected with P1 and P56 ATAC-seq cardiomyocyte datasets. Chromatin accessibility was unaltered around these target gene promoters during cardiomyocyte development. ATAC-seq datasets obtained from (Quaife-Ryan et al., 2017) (GSE95764). For each ATAC-seq, n = 3.

Table S1. Antibodies used in this study

Antibody	Species	Samples	Company	Cat No	Dilution
Alexa Fluor 488 goat anti-chicken IgG (H+L)	Goat IgG	Secondary antibody	Life Technologies	A-11039	1:33
Alexa Fluor 488 goat anti-mouse IgG (H+L)	Goat IgG	Secondary antibody	Life Technologies	A-11029	1:10
Alexa Fluor 488 goat anti-mouse IgM (μ chain)	Goat IgG	Secondary antibody	Life Technologies	A-21042	1:33
Alexa Fluor 488 goat anti-rabbit IgG (H+L)	Goat IgG	Secondary antibody	Life Technologies	A-11034	1:67
Alexa Fluor 555 goat anti-mouse IgG (H+L)	Goat IgG	Secondary antibody	Life Technologies	A-21422	1:100
Alexa Fluor 555 goat anti-rabbit IgG (H+L)	Goat IgG	Secondary antibody	Life Technologies	A-21428	1:100
Alexa Fluor 633 goat anti-rabbit IgG (H+L)	Goat IgG	Secondary antibody	Life Technologies	A-21070	1:100
anti-BrdU	IgG1, kappa light chain	IF imaging	DSHB	G3G4 (anti-BrdU)	1:100
Anti-MLC-2v	Rabbit IgG	IF imaging	Proteintech	10906-1-AP	1:1000
Anti-phospho-Histone H3 (Ser10)	Rabbit polyclonal	IF imaging	Millipore	06-570	1:100
Anti-TnTc	Mouse IgG1	IF imaging	Thermo Scientific	MS-295-P0	1:100
anti-β-catenin (PY489)	Mouse IgM	IF imaging	DSHB	PY489-B-catenin	1:400
CD31-BV421	Rat IgG2a	Mouse FACS	BioLegend	102423	1:100
CD45-FITC	Rat IgG2b	Mouse FACS	Miltenyi Biotec	130-102-778	1:200
CD90	Mouse IgG2A	hPSC FACS	RnD Systems	MAB2067	1:400
CD90-APC	Rat IgG2c	Mouse FACS	ThermoFisher	A14727	1:400
GFP	Chicken polyclonal	IF imaging	Abcam	ab13970	1:400
Ki-67 (D3B5)	Rabbit IgG	IF imaging	Cell Signalling Technology	9129	1:400
Podoplanin-PE/Cy7	Syrian Hamster IgG	Mouse FACS	BioLegend	127411	1:400
Wheat germ agglutinin, Alexa Fluor 488	NA	IF imaging	ThermoFisher Scientific	W11261	1:400
α-Actinin (clone EA-53)	Mouse IgG1	IF imaging	ThermoFisher	A-21070	1:400

Table S2 Primers for quantitative PCR

Gene	Accession	Forward	Reverse	Size (bp)
Human qPCR primers				
18s	18s repeat sequence	TCGAGGCCCTGTAATTGGAA	CCCTCCAATGGATCCTCGTT	61
COL1a1	ENSG00000108821	GTGCTAAAGGTGCCAATGGT	ACCAGGTTCACCGCTGTTAC	128
HPRT1	ENSG00000165704	AACCTCTCGGCTTTCCCG	TCACTAATCACGACGCCAGG	150
MYH6	ENSG00000197616	CTCCTCCTACGCAACTGC	ACACCGTCTGGAAGGATGA	83
CTNNB1	ENSG00000168036	CTTACACCCACCATCCCACT	TGATGTGCACGAACAAGCAA	144
Mouse qPCR primers				
18s	18s repeat sequence	TCGAGGCCCTGTAATTGGAA	CCCTCCAATGGATCCTCGTT	61
Anln	ENSMUSG00000036777	ATGTTAGTGGCTTTGGTGCC	TGGGATTCTTTCGCCTCTCA	102
Birc5	ENSMUSG00000017716	AACCCGATGACAACCCGAT	TGGTCTCCTTTGCAATTTTGTTC	150
Cdk1	ENSMUSG00000019942	ACACACACGAGGTAGTGACG	AACCGGAGTGGAGTAACGAG	80
Depdc1b	ENSMUSG00000021697	TTGTGATTCAAACTGCGGCG	TCCACTGTTTCATTCCACAGC	143
E2f1	ENSMUSG00000027490	ACCCAGGGAAAGGTGTGAAA	CAAGAAGCGTTTGGTGGTCA	80
Hprt	ENSMUSG00000025630	AGGCCAGACTTTGTTGGATTTGAA	CAACTTGCGCTCATCTTAGGCTTT	150
Iqgap3	ENSMUSG00000028068	GAGCTCGGACAGCCTATGAGC	AGCCGGCAGAGGTACTGATA	88
Kif18a	ENSMUSG00000027115	GTGGATTTGCCAAACGCATTC	TTTATAGCCCACTTTCAGTCTGT	80
Kif4	ENSMUSG00000034311	CCAGCAAACAGAAACCCCAT	AAGGTTTGGGCTTAGGTGGA	87
Klf15	ENSMUSG00000030087	GGAGAGCGGGGAGAGC	TGTGGTGACTGGACTCCG	148
Mad2l1	ENSMUSG00000029910	GAAGAATCGGGACCGCAA	CAGACCAAACGAACCGTCTC	138
Plk4	ENSMUSG00000025758	CGTAGAGAAGGCGTCCTGAT	TAAAGTCCTCGATCCTCTCCC	143
Ppargc1a	ENSMUSG00000029167	CTCTCAGTAAGGGGCTGGTT	CAGCACACTCTATGTCACTCC	150
Pttg1	ENSMUSG00000020415	TGGCGCAGTCTTCGAGTAAT	ATCCTTAGATGCCAAACGGC	91
Miscellaneous qPCR Primers				
GFP	-	AAGGGCATCGACTTCAAGG	TGCTTGTCGGCCATGATATAG	95

Table S3 Summary of RNA-seq mapping efficiencies of MIP56 caBCAT experiment

Sample	number of reads	%uniquely mapped reads	%multi-mapped reads	%unmapped
Myo_GFP_1	65812645	71.21%	25.52%	3.27%
Myo_GFP_2	58613420	69.79%	26.80%	3.41%
Myo_GFP_3	67027367	71.61%	24.98%	3.41%
Myo_GFP_4	65004587	71.52%	24.60%	3.88%
Myo_BCAT_1	71693147	71.26%	25.37%	3.37%
Myo_BCAT_2	74057324	73.35%	23.83%	2.82%
Myo_BCAT_3	67597492	70.32%	26.50%	3.18%
Myo_BCAT_4	65687633	69.98%	26.81%	3.21%

Table S4 Summary of mapping efficiencies for ChIP-seq

Sample	number of reads	%uniquely mapped reads	%multi-mapped reads	%unmapped
H3K27ac_1	40192146	69.93%	28.52%	1.55%
H3K27ac_2	73153197	76.80%	22.26%	0.94%
H3K4me3_1	42817370	67.22%	31.03%	1.74%
H3K4me3_2	71856079	75.62%	22.83%	1.54%
Input_1	82802143	71.20%	27.28%	1.53%
Input_2	85319259	73.57%	24.84%	1.59%
TCF7l2_1	66744568	68.12%	29.74%	2.09%
TCF7l2_2	77627877	68.35%	28.43%	3.22%

Table S5. Bioinformatic programs used in this study

Software	Reference	RRID
NCBI Primer-BLAST	(Ye et al., 2012)	RRID:SCR_003095
Trimmomatic	(Bolger et al., 2014)	RRID:SCR_011848
STAR	(Dobin et al., 2013)	RRID:SCR_015899
HTSeq-count	(Anders et al., 2015)	RRID:SCR_011867
EdgeR	(Robinson et al., 2010)	RRID:SCR_012802
DAVID	(Huang et al., 2007)	RRID:SCR_001881
GENE-E	Broad Institute	N/A
Bowtie2	(Langmead and Salzberg, 2012)	RRID:SCR_005476
MACS2	(Zhang et al., 2008)	RRID:SCR_013291
GenomicRanges	(Lawrence et al., 2013)	RRID:SCR_000025
deepTools2	(Ramírez et al., 2016)	RRID:SCR_016366
GREAT	(McLean et al., 2010)	RRID:SCR_005807
HOMER	(Heinz et al., 2010)	RRID:SCR_010881

References:

Anders, S., Pyl, P. T. and Huber, W. (2015). HTSeq--a Python framework to work with high-throughput sequencing data. *Bioinformatics* **31**, 166-169.

Arner, E., Daub, C. O., Vitting-Seerup, K., Andersson, R., Lilje, B., Drabløs, F., Lennartsson, A., Rönnerblad, M., Hrydziuszko, O., Vitezic, M., et al. (2015). Gene regulation. Transcribed enhancers lead waves of coordinated transcription in transitioning mammalian cells. *Science (New York, N.Y.)* **347**, 1010-1014.

Bolger, A. M., Lohse, M. and Usadel, B. (2014). Trimmomatic: a flexible trimmer for Illumina sequence data. *Bioinformatics* **30**, 2114-2120.

Dobin, A., Davis, C. A., Schlesinger, F., Drenkow, J., Zaleski, C., Jha, S., Batut, P., Chaisson, M. and Gingeras, T. R. (2013). STAR: ultrafast universal RNA-seq aligner. *Bioinformatics* **29**, 15-21.

Heinz, S., Benner, C., Spann, N., Bertolino, E., Lin, Y. C., Laslo, P., Cheng, J. X., Murre, C., Singh, H. and Glass, C. K. (2010). Simple combinations of lineage-determining transcription factors prime cis-regulatory elements required for macrophage and B cell identities. *Molecular Cell* **38**, 576-589.

Huang, D. W., Sherman, B. T., Tan, Q., Collins, J. R., Alvord, W. G., Roayaei, J., Stephens, R., Baseler, M. W., Lane, H. C. and Lempicki, R. A. (2007). The DAVID Gene Functional Classification Tool: a novel biological module-centric algorithm to functionally analyze large gene lists. *Genome biology* **8**, R183-116.

Langmead, B. and Salzberg, S. L. (2012). Fast gapped-read alignment with Bowtie 2. *Nature Methods* **9**, 357-359.

Lawrence, M., Huber, W., Pagès, H., Aboyoun, P., Carlson, M., Gentleman, R., Morgan, M. T. and Carey, V. J. (2013). Software for computing and annotating genomic ranges. *PLoS computational biology* **9**, e1003118.

McLean, C. Y., Bristor, D., Hiller, M., Clarke, S. L., Schaar, B. T., Lowe, C. B., Wenger, A. M. and Bejerano, G. (2010). GREAT improves functional interpretation of cis-regulatory regions. *Nature Biotechnology* **28**, 495-501.

Quaife-Ryan, G. A., Sim, C. B., Ziemann, M., Kaspi, A., Rafehi, H., Ramialison, M., El-Osta, A., Hudson, J. E. and Porrello, E. R. (2017). Multicellular Transcriptional Analysis of Mammalian Heart Regeneration. *Circulation* **136**, 1123-1139.

Ramírez, F., Ryan, D. P., Grüning, B., Bhardwaj, V., Kilpert, F., Richter, A. S., Heyne, S., Dündar, F. and Manke, T. (2016). deepTools2: a next generation web server for deep-sequencing data analysis. *Nucleic acids research* **44**, W160-165.

Robinson, M. D., McCarthy, D. J. and Smyth, G. K. (2010). edgeR: a Bioconductor package for differential expression analysis of digital gene expression data. *Bioinformatics* **26**, 139-140.

Spurrell, C. H., Barozzi, I., Mannion, B. J., Blow, M. J., Fukuda-Yuzawa, Y., Afzal, S. Y., Akiyama, J. A., Afzal, V., Tran, S., Plajzer-Frick, I., et al. (2019). Genome-Wide Fetalization of Enhancer Architecture in Heart Disease. *bioRxiv*, 591362.

Visel, A., Blow, M. J., Li, Z., Zhang, T., Akiyama, J. A., Holt, A., Plajzer-Frick, I., Shoukry, M., Wright, C., Chen, F., et al. (2009). ChIP-seq accurately predicts tissue-specific activity of enhancers. *Nature* **457**, 854-858.

Ye, J., Coulouris, G., Zaretskaya, I., Cutcutache, I., Rozen, S. and Madden, T. L. (2012). Primer-BLAST: A tool to design target-specific primers for polymerase chain reaction. *BMC Bioinformatics* **13**, 134.

Zhang, Y., Liu, T., Meyer, C. A., Eeckhoute, J., Johnson, D. S., Bernstein, B. E., Nusbaum, C., Myers, R. M., Brown, M., Li, W., et al. (2008). Model-based analysis of ChIP-Seq (MACS). *Genome biology* **9**, R137.